Atmos. Chem. Phys., 24, 12943–12962, 2024
https://doi.org/10.5194/acp-24-12943-2024

Atmospheric Chemistry and Physics
Open Access
EGU

Research article

The atmospheric oxidizing capacity in China – Part 2: Sensitivity to emissions of primary pollutants

Jianing Dai[1], Guy P. Brasseur[1,5,6], Mihalis Vrekoussis[2,7,8], Maria Kanakidou[2,4], Kun Qu[2], Yijuan Zhang[2], Hongliang Zhang[3], and Tao Wang[6]

[1]Environmental Modelling Group, Max Planck Institute for Meteorology, 20146 Hamburg, Germany
[2]Institute of Environmental Physics (IUP), University of Bremen, 28359 Bremen, Germany
[3]Department of Environmental Science and Engineering, Fudan University, 200433 Shanghai, China
[4]Environmental Chemical Processes Laboratory, Department of Chemistry, University of Crete, 70013 Heraklion, Greece
[5]NSF-National Center for Atmospheric Research, Boulder, CO 80307, USA
[6]Department of Civil and Environmental Engineering, The Hong Kong Polytechnic University, Hong Kong SAR, China
[7]Center of Marine Environmental Sciences (MARUM), University of Bremen, 28359 Bremen, Germany
[8]Climate and Atmosphere Research Center (CARE-C), The Cyprus Institute, 2121 Nicosia, Cyprus

Correspondence: Guy P. Brasseur (guy.brasseur@mpimet.mpg.de)

Received: 7 March 2024 – Discussion started: 26 March 2024
Revised: 13 September 2024 – Accepted: 25 September 2024 – Published: 21 November 2024

Abstract. Despite substantial reductions in anthropogenic emissions, ozone (O_3) pollution remains a severe environmental problem in urban China. These reductions affect ozone formation by altering levels of O_3 precursors, intermediates, and the oxidation capacity of the atmosphere. However, the underlying mechanisms driving O_3 changes are still not fully understood. Here, we employ a regional chemical transport model to quantify ozone changes due to a specified emission reduction (50 %) for winter and summer conditions in 2018. Our results indicate that reductions in nitrogen oxide (NO_x) emissions increase surface O_3 concentrations by 15 %–33 % on average across China in winter and by up to 17 % in volatile organic compound (VOC)-limited areas during summer. These ozone increases are associated with a reduced NO_x titration effect and higher levels of OH radicals. Reducing NO_x emissions significantly decreases the concentration of particulate nitrate, which enhances ozone formation through increased HO_2 radical levels due to reduced aerosol uptake and diminished aerosol extinction. Additionally, an enhanced atmospheric oxidative capacity, driven by larger contributions from the photolysis of oxidized VOCs (OVOCs) and OH-related reactions, also favors urban ozone formation. With additional reductions in anthropogenic VOC emissions, increases in summertime ozone (VOC-limited areas) can be offset by reduced production of radicals from VOC oxidations. To effectively mitigate ozone pollution, a simultaneous reduction in the emission of NO_x and specific VOC species should be applied, especially regarding alkenes, aromatics, and unsaturated OVOCs, including methanol and ethanol.

Published by Copernicus Publications on behalf of the European Geosciences Union.

1 Introduction

To effectively reduce air pollution in China, the government of the country implemented stringent actions between 2013 and 2020 (Liu and Wang, 2020; Liu et al., 2023). In the initial phase, from 2013 to 2017, the control of primary pollutants was particularly effective, with a dramatic decrease in the anthropogenic emissions of fine particles ($PM_{2.5}$), sulfur dioxide (SO_2), and nitrogen oxides (NO_x) (Zheng et al., 2018; Liu and Wang, 2020). In subsequent years, a sustained reduction in the emissions of SO_2, NO_x, and $PM_{2.5}$ was achieved, particularly between 2018 and 2020 (Liu et al., 2023). The implementation of these emission control policies has greatly improved China's air quality. However, a significant increase in the surface ozone (O_3) concentration was observed from 2013 to 2019, with the positive trend slowing down in 2020 and 2021 but rebounding in 2022 (Liu et al., 2023; China Air, 2023). Several studies provide explanations for the positive trend observed in the surface O_3 concentration, including a reduction in the NO_x emissions and the atmospheric aerosol load (Li et al., 2019; Liu and Wang, 2020). During and after the recent COVID-19 lockdown period, ozone pollution was reported as happening, which is believed to be favored by a sharp reduction in NO_x and high emissions of volatile organic compounds (VOCs) (K. Li et al., 2021). Looking through these changes over the past decade, we learn that rapid reductions in emissions disturb ozone chemistry substantially and, thereby, produce changes in ozone concentrations.

The response of ozone to reduced NO_x emissions varies with the local photochemical environment and specifically with the encountered chemical regimes (i.e., VOC-limited, NO_x-limited, or transition conditions) (Jacob et al., 1995; Ou et al., 2016; Dai et al., 2023). In NO_x-sensitive regimes, the reduction in NO_x emissions decreases the number of NO_2 molecules photolyzed, leading to fewer ozone molecules being produced, while in VOC-sensitive regimes the reduction in the NO_x abundance tends to enhance the ozone formation due to the weakening of NO titration and the reduced loss of the OH radical by the reaction with NO_2. Several studies based on satellite observations (Wang et al., 2021) and regional models (Zhu et al., 2023) have shown that the reduction in anthropogenic emissions has generated a change in the geographical distribution of the ozone formation regimes in China. These studies have reported a shift in ozone sensitivity regimes from VOC-sensitive to transition and/or even to NO_x-sensitive in many metropolitan and suburban regions of East China. The shift towards NO_x-limited conditions facilitates the implementation of an efficient ozone control through the reduction in NO_x emissions only. In the remaining VOC-sensitive and transition areas, NO_x emission reduction fails to effectively mitigate ozone pollution. In this situation, a coordinated reduction in anthropogenic VOC (AVOC) emissions should be implemented to effectively limit the ozone formation (Liu et al., 2023; Zhu et al., 2023). The source of NO_x in VOC-sensitive areas is mainly from fossil fuel combustion, while the emissions of AVOCs result from a broad range of industrial, transportation, and residential sources (B. Li et al., 2021; C. Li et al., 2022). To establish a cost-effective control over AVOC emissions, the contribution of different VOC categories to ozone formation should be accurately quantified for different areas of China.

The effect of aerosols on the O_3 formation has been considered in several modeling studies (Li et al., 2019; Liu and Wang, 2020). However, the influences of aerosol on the ozone production are complex due to the different effects that must be taken into consideration (Tan et al., 2022; Dai et al., 2023). Understanding the changes in aerosol effects on the O_3 formation, when the primary emissions are reduced further, remains a necessity for implementing successful air quality control policies.

Recent observational studies combined with a source apportionment approach using observation-based models have highlighted the role of anthropogenic VOC species, including alkenes, aromatics, and oxidized VOCs (OVOCs), in mitigating summertime ozone formation in urban areas in China (C. Li et al., 2022; W. Wang et al., 2022). The notable contributions of OVOCs to the atmospheric oxidizing capacity (AOC) and the formation of secondary organic aerosols (SOA) have been a concern in the regions of the Yangtze River Delta (YRD) (J. Li et al., 2022) and the Pearl River Delta (PRD) (W. Wang et al., 2022). The important role of biogenic VOCs (BVOCs) has also been highlighted in vegetated rural and urban regions in China, where the oxidation of BVOCs can significantly contribute to the formation of ozone and aerosols, specifically in the PRD region (Wang et al., 2023; Zhang et al., 2023). However, a comprehensive evaluation of the changes in the contributions of the different VOC categories to AOC and the ozone chemistry in response to emission changes in the different regions of China is still needed. Considering the necessity of implementing coordinated actions in several large geographical areas to further alleviate air pollution in China, regional chemical transport models are appropriate tools for assessing the quantitative response of secondary pollutants and the oxidizing capacity of the atmosphere for emission changes.

In the companion paper (Part 1; Dai et al., 2023), we use a regional chemical–meteorological model to quantify the relative contributions of different photochemical processes to the formation and destruction of near-surface photochemical radicals and ozone in different chemical environments in China. In this study (Part 2), with the evaluated model, we assess the response of the photo-oxidative species and related parameters to an imposed reduction in the primary emissions. This paper is structured as follows. Section 2 introduces the setup of the model system and describes the simulations performed for specified reduction scenarios in the emissions of primary pollutants. In Sect. 3, we analyze the response of near-surface concentrations of ozone to the specified emission reductions. Further, we determine the drivers responsi-

ble for the resulting ozone changes; these include changes in the concentrations of ozone precursors, intermediates including the OVOCs, and the levels of secondary aerosols. We also discuss the changes to be expected in the ozone formation regimes. Finally, we describe the sensitivity of the AOC to the reduction in the emissions. A summary and implication for the policy-making of our study are provided in Sect. 4.

2 Method

2.1 Model setting

We use the Weather Research and Forecasting model with Chemistry (WRF-Chem) version 4.1.2 (Skamarock et al., 2019), coupled with the gas-phase chemistry mechanism MOZART (Emmons et al., 2010) and the aerosol module MOSAIC (Zaveri et al., 2008), to simulate the meteorological fields, transport, and chemical and physical transformations of trace gases and aerosols. The months of January and July 2018 are selected as representative months to conduct the simulations and to investigate the changes in secondary pollution and in the AOC in response to emission reductions during winter and summer, respectively. Compared to the standard version of the chemical mechanism, several updates of heterogeneous uptake on the surface of the ambient aerosol were implemented (Dai et al., 2023). As for the SOA formation, the main pathways result from the gas-phase oxidation of VOCs by atmospheric oxidants (OH, O_3, and NO_3) and from the heterogeneous formation of glyoxal SOA over the ambient aerosol (Knote et al., 2014). The model domain covers the whole geographical area of China. Analyses of modeling results at four urban sites (Beijing, Shanghai, Guangzhou, and Chengdu) are also performed. More detailed information on the model configuration, the model validation, and the sites selected for our analysis can be found in Part 1 of our paper (Dai et al., 2023).

We adopt the Multi-resolution Emission Inventory for China (MEIC v1.3; http://www.meicmodel.org/, last access: 7 March 2024) to represent anthropogenic emissions in China and the CAMS-GLOB-ANT v4.2 inventory (https://eccad.aeris-data.fr/, last access: 7 March 2024) provided by the Copernicus Atmosphere Monitoring Service (CAMS) to account for the anthropogenic emissions in the Asian areas outside China. To explore the sensitivity of secondary pollution and the AOC to emission reduction, several sensitivity experiments are designed based on our emission inputs of NO_x and AVOCs. As shown in Table S1 in the Supplement, NO_x emissions include those of NO_2 and NO, and AVOC emissions include those of alkanes (ethane C_2H_6, propane C_3H_8, and BIGALK – alkanes with carbon number ≥ 4), alkenes (ethene C_2H_4, propene C_3H_6, and BIGENE – alkenes with carbon number ≥ 4), aromatics (benzene C_6H_6, toluene $C_6H_5CH_3$, and xylene $C_6H_4(CH_3)_2$)), alkyne (C_2H_2), isoprene (C_5H_8), terpenes ($C_{10}H_{16}$), and OVOCs (methanol CH_3OH, ethanol C_2H_5OH, acetaldehyde CH_3CHO, acetone CH_3COCH_3, methacrolein CH_2CCH_3CHO/MACR, and methyl vinyl ketone $CH_2CHCOCH_3$/MVK). Emissions of ammonia (NH_3), sulfur dioxide (SO_2), and carbon monoxide (CO) are also considered.

2.2 Design of the numerical experiment

To explore the sensitivity of secondary pollutants to emission changes, five numerical experiments are conducted for January and July 2018, respectively (Table 1). In the baseline case, denoted as *BASE*, we adopt the emissions described in Sect. 2.1. The concentrations of the key species calculated in this specific case have been validated in our companion study (Part 1, Dai et al., 2023). To quantify the sensitivity of pollutants to potential mitigation policies, we apply uniform reductions in the surface emissions of primary pollutants over the entire geographical area of China. In the first two cases, arbitrary 50 % reductions are applied separately to the NO_x and AVOC emissions relative to the baseline case. These two cases are labeled *NOx* and *AVOCs*, respectively. A third case in which the 50 % reduction is applied to both NO_x and AVOC emissions is referred to as $N + A$. The difference between the "perturbed" concentrations of pollutants and chemical parameters relative to the baseline case provides an estimate of the response of secondary pollution and chemistry to emission reduction.

Additionally, a simulation labeled *TOTAL* assumes that all the anthropogenic emissions under consideration (NO_x, AVOCs, CO, SO_2, and NH_3) are simultaneously reduced by 50 %. This particular case is used to explore the impact on the ozone formation of a reduction in the emission of CO (an ozone precursor) and of SO_2 and NH_3 (as aerosol precursors). The spatial distribution of the changes in the emission fluxes for the different cases is shown in Fig. S1 in the Supplement.

3 Model results

3.1 Response of ozone concentrations to emission reduction

First, we describe the changes in the surface concentration of ozone in response to the reduction applied to the surface emissions. To support the discussion, we adopt an indicator to distinguish between different ozone sensitivity regimes. This indicator is defined as the calculated ratio between the production rates of hydrogen peroxide (H_2O_2) and nitric acid (HNO_3) [$P(H_2O_2)/P(HNO_3)$]. An area is assumed to be VOC-limited or NO_x-limited if the adopted indicator $P(H_2O_2)/P(HNO_3)$ is smaller than 0.06 or larger than 0.2 (Tonnesen and Dennis, 2000; Yang et al., 2020; Zhao et al., 2019; Dai et al., 2023). The regions with ratios between these two limits represent transition situations.

Table 1. Sensitivity experiments.

Model experiment	Description*
BASE	Without emission reduction
NOx	With emission reduction in NO_x by a factor of 2
AVOCs	With emission reduction in anthropogenic VOCs by a factor of 2
$N + A$	With emission reduction in NO_x and anthropogenic VOCs by a factor of 2
TOTAL	With emission reduction in all considered species by a factor of 2

* The relevant species in emission inputs are shown in Sect. 2.1 and Table S1.

Figure 1 displays the spatial distribution of the changes in the surface concentrations of ozone during daytime (06:00 to 19:00 local standard time – LST) resulting from a 50 % reduction in the emissions of NO_x, AVOCs, combined NO_x and AVOCs, and other anthropogenic species (NH_3, SO_2, and CO) for January and July 2018.

Winter conditions. In January, the 50 % reduction in the NO_x emissions (*NOx* case) enhances the surface ozone concentrations, with the largest increase of 15 %–33 % (6–12 ppbv; Fig. 1a) found in the YRD and PRD regions. During wintertime, a large part of China is under a VOC-sensitive regime (Fig. S2a). The reduced ozone titration due to NO_x emission reduction leads to a decrease in ozone destruction (Fig. S3a) and hence favors an increase in the ozone concentration. If AVOC emissions are reduced by 50 % (*AVOCs* case), the surface ozone concentration is reduced by 4 %–10 % (2.0–8.0 ppbv; Fig. 1b) in South China. This ozone decrease is associated with reduced levels of radicals (see Sect. 3.2.1) and hence a reduction in the ozone production (Fig. S4a).

In the case with a combined emission reduction ($N + A$ case), the ozone response in VOC-limited areas follows the positive changes found in the NO_x reduction case, with an ozone increase of 4 %–9 % (3.0–7.5 ppbv; Fig. 1c) in North China and in some urban regions in South China. Simultaneously, a slight decrease in the ozone concentration is derived along the coast of South China (5 %–8 % or 2.0–4.5 ppbv). In these areas, the ozone sensitivity is under the control of the NO_x. The ozone decrease is dominated by the negative ozone response to the AVOC emission reduction. With a further emission reduction for the other chemical species (*TOTAL* case), an ozone increase (4 %–6 % or 3–5 ppbv; Fig. 1d) relative to the combined case is calculated for South China.

Summer conditions. In July, with the reduction in the NO_x emissions, an increase in the surface ozone concentration of up to 17 % (10 ppbv; Fig. 1e) is calculated in the urbanized regions of the North China Plain (NCP), the YRD, and the PRD. These areas are typically VOC-limited (Fig. S2b); thus, the ozone increase is explained by the reduced ozone titration due to NO_x emission reduction. At the same time, in NO_x-limited areas, the calculated surface ozone concentration is reduced by 3 %–10 % (2–8 ppbv) in response to the reduced photochemical formation under lower NO_x concentrations. With the reduction in AVOC emissions, the surface concentration of ozone decreases by 8 %–20 % (8.0–12.0 ppbv; Fig. 1f) in all the areas of China.

In the combined emission reduction case, the surface concentration of ozone decreases by up to 15 % (12 ppbv; Fig. 1g) in the NO_x-sensitive areas. In the VOC-sensitive areas, the surface ozone concentration also decreases, which differs from the ozone changes derived for winter conditions. This is explained by the fact that the loss of ozone due to NO_x titration is rapidly compensated for by the photochemical formation of ozone, as the ozone production rate is enhanced by high temperatures and by high photolysis rates during summertime (T. Wang et al., 2022). When the emission reduction is applied to all species under consideration, the ozone changes (Fig. 1h) relative to the combined case are smaller than the changes derived in winter, due to a consistently smaller reduction in aerosol concentrations (see Sect. 3.2.3).

Table 2 and Fig. S5 provide quantitative information on the response of ozone to emission reduction at four urban locations (Beijing, Shanghai, Chengdu, and Guangzhou) for January and July 2018. In winter (in January), the reduction in the emission of NO_x results in ozone increases of 21.3 %–33.2 % in all the cities, while the reduction applied to AVOC emissions results in a decrease in urban ozone levels of 2.5 %–18.2 %. Ozone changes in the $N + A$ and *TOTAL* cases follow the ozone response found in the *NOx* case, with concentration increases of 7.1 %–22.0 % and 10.0 %–22.7 %, respectively. In summer (in July), the urban ozone responses to the *NOx* and *AVOCs* cases are similar to those derived for winter conditions. The calculated ozone concentrations increase by 5.5 %–17.1 % in response to the reduced NO_x emissions and decrease by 14.5 %–22.9 % in response to the reduced AVOC emissions. In the $N + A$ and *TOTAL* cases, the changes in the ozone concentration follow the responses to the AVOC reductions: the ozone concentration decreases at the Beijing (by 5.5 % and 7.3 %), Shanghai (by 2.9 % and 2.6 %), and Chengdu (by 3 % and 2.5 %) sites. An exception is found at the Guangzhou site, where the ozone concentration increases by 1.3 % in both cases; this indicates a different role of the anthropogenic emissions in the ozone formation at this location.

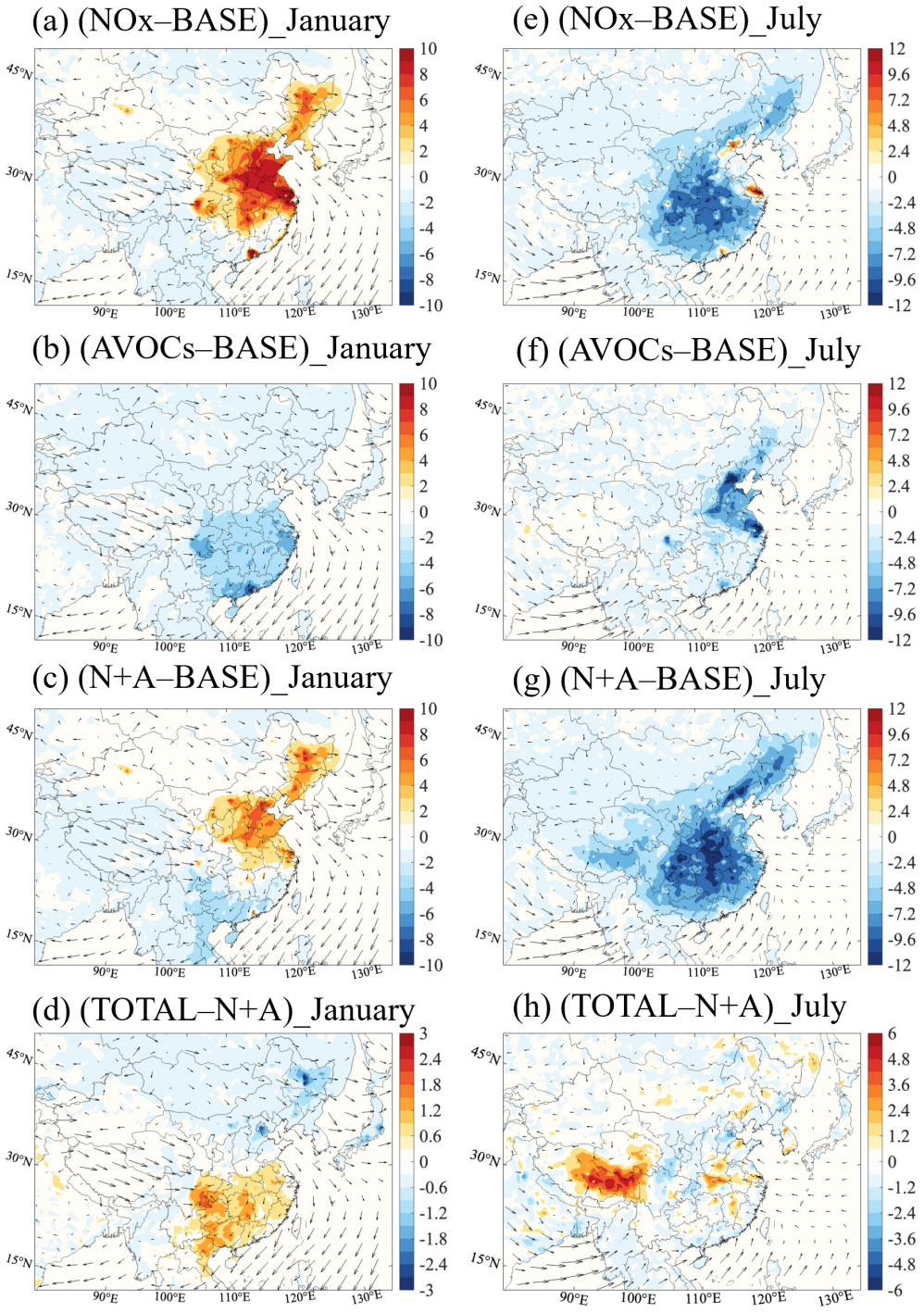

Figure 1. Changes in the monthly averaged daytime (06:00 to 19:00 LST) surface ozone concentration (ppbv) response to a 50 % reduction in NO_x emissions (**a, e**; *NOx* case), anthropogenic VOC (AVOC) emissions (**b, f**; *AVOCs* case), and combined NO_x and AVOC emissions (**c, g**; $N + A$ case) relative to the *BASE* case. Additional reduction in the emission of CO, NH_3, and SO_2 by 50 % (**d, h**; *TOTAL* case) and relative to the $N + A$ case for January **(a–d)** and July **(e–h)** 2018. The arrows represent the wind speed and wind direction. Note the inconsistency in the scale of panels **(d)** and **(h)**.

Table 2. Percentage changes in surface ozone due to emission reduction in urban locations.

Location	Site	Ozone changes under winter conditions (mean ± SD)			
		NOx[a]	*AVOCs*[b]	$N+A$[c]	*TOTAL*[d]
North	Beijing	25.0 ± 25.2[e]	−2.5 ± 1.3	22.0 ± 32.8	20.0 ± 19.5
East	Shanghai	33.2 ± 35.3	−18.2 ± 13.5	21.8 ± 20.5	22.7 ± 18.8
South	Guangzhou	21.4 ± 22.6	−17.1 ± 11.2	7.1 ± 3.2	10.0 ± 3.5
West	Chengdu	21.3 ± 23.8	−9.4 ± 8.5	14.1 ± 8.3	20.3 ± 13.5
Location	Site	Ozone changes under summer conditions (mean ± SD)			
		NOx	*AVOCs*	$N+A$	*TOTAL*
North	Beijing	6.4 ± 3.8	−21.8 ± 19.2	−5.5 ± 4.2	−7.3 ± 5.0
East	Shanghai	17.1 ± 12.8	−22.9 ± 20.8	−2.9 ± 2.1	−2.6 ± 1.5
South	Guangzhou	15.0 ± 13.1	−14.5 ± 13.5	1.3 ± 1.0	1.3 ± 0.9
West	Chengdu	5.5 ± 4.5	−14.5 ± 10.2	−5.5 ± 2.0	−4.5 ± 1.9

[a–d] Sensitivity cases with a 50 % reduction in emissions of the NO_x (*NOx*), AVOCs (*AVOCs*), NO_x and AVOCs ($N+A$), and other species (NO_x, AVOCs, CO, NH_3, and SO_2) under consideration (*TOTAL*).
[e] Values are displayed as percentage average ozone changes during daytime (06:00 to 19:00 LST), with the standard deviation as the error bar (ozone changes = (case value − base value) / base value × 100).

3.2 Changes in precursors and intermediates in ozone formation

In this section, we describe changes in the surface concentrations of ozone precursors and intermediates in response to the reduction in surface emissions. We focus in particular on the hydroxyl radical (OH), the hydroperoxyl radical (HO_2), specific OVOC species, and secondary aerosols.

3.2.1 Changes in radicals

To support the discussion on the radical changes induced by the emission reduction, we examine the changes in the values of two specific parameters: the production rate of peroxy radicals ($RO_x = OH + HO_2 + RO_2$; $P(RO_x)$) and the destruction rate of these radicals ($D(RO_x)$) (Tan et al., 2019). The production rate of RO_x radicals ($P(RO_x)$) includes the photolysis of O_3, nitrous acid (HONO), and different OVOC species as well as the ozonolysis of alkenes. The destruction rate of RO_x radicals ($D(RO_x)$) results from the termination reactions between different RO_x radicals and between RO_x radicals and nitric oxide. Another loss process for hydroperoxy radicals is provided by the heterogeneous uptake of HO_2 on aerosol surfaces. Detailed model estimates of $P(RO_x)$ and $D(RO_x)$ can be found in Part 1 of the present study (Dai et al., 2023).

Winter conditions. Figure 2 displays the spatial distribution of the changes in the surface daytime (06:00 to 19:00 LST) mixing ratios of OH and HO_2 radicals resulting from a 50 % reduction in the emissions of NO_x, AVOCs, combined NO_x and AVOCs, and additional species (NH_3, SO_2, and CO) for January 2018. With the reduction in NO_x emissions (*NOx* case), the calculated mixing ratio of the surface OH radical is reduced in South China by up to 40 % (0.05 pptv; Fig. 2a), with a lower decrease in the central and western parts of the country. The reduction in the levels of the OH radical are due to the reduced oxidative capacity of the atmosphere associated with the NO_x emission reduction. The reduction in the atmospheric oxidative capacity is attributable to the decreases in the concentrations of NO_2 (Fig. S6a) and ozone.

At the same time, an increase in the mixing ratios of OH radicals is found in urban areas, including the NCP, YRD, PRD, and Sichuan Basin (SCB) regions, with a maximum increase of 24 % in the PRD region. Consistently, at the four city sites under consideration, the highest increase in the level of the OH radical is found at the Guangzhou site (Fig. S7). This increase results from the reduced loss of the OH radical through the reaction with NO_2 (Fig. S6b).

A distinct increase in the surface mixing ratio of the HO_2 radical is derived in South China: it reaches 5 pptv or 60 % (Fig. 2e). This increase contributes to a higher ozone level through the reaction between HO_2 and NO. The enhancement in the urban HO_2 concentration results from the increased levels of the OH radical via VOC oxidation. The reduction in the aerosol load derived in South China as a result of the reduced NO_x emission is responsible for the reduced loss of HO_2 by aerosol uptake (see Sect. 3.2.3).

For the 50 % decrease in AVOC emissions (*AVOCs* case), the mixing ratios of OH and HO_2 radicals are reduced in South China by 4 %–12 % (0.005–0.015 pptv; Fig. 2b) and 20 %–36 % (1–3 pptv; Fig. 2f), respectively. The decrease in the levels of these radicals is related to the reduced oxidation rates of VOCs following the decrease in the emissions and hence in the concentrations of hydrocarbons (Fig. S8a). The production of RO_x also decreases, especially from the reduced photolysis of formaldehyde (HCHO) and other OVOCs (Fig. S8b, c), which is a consequence of the

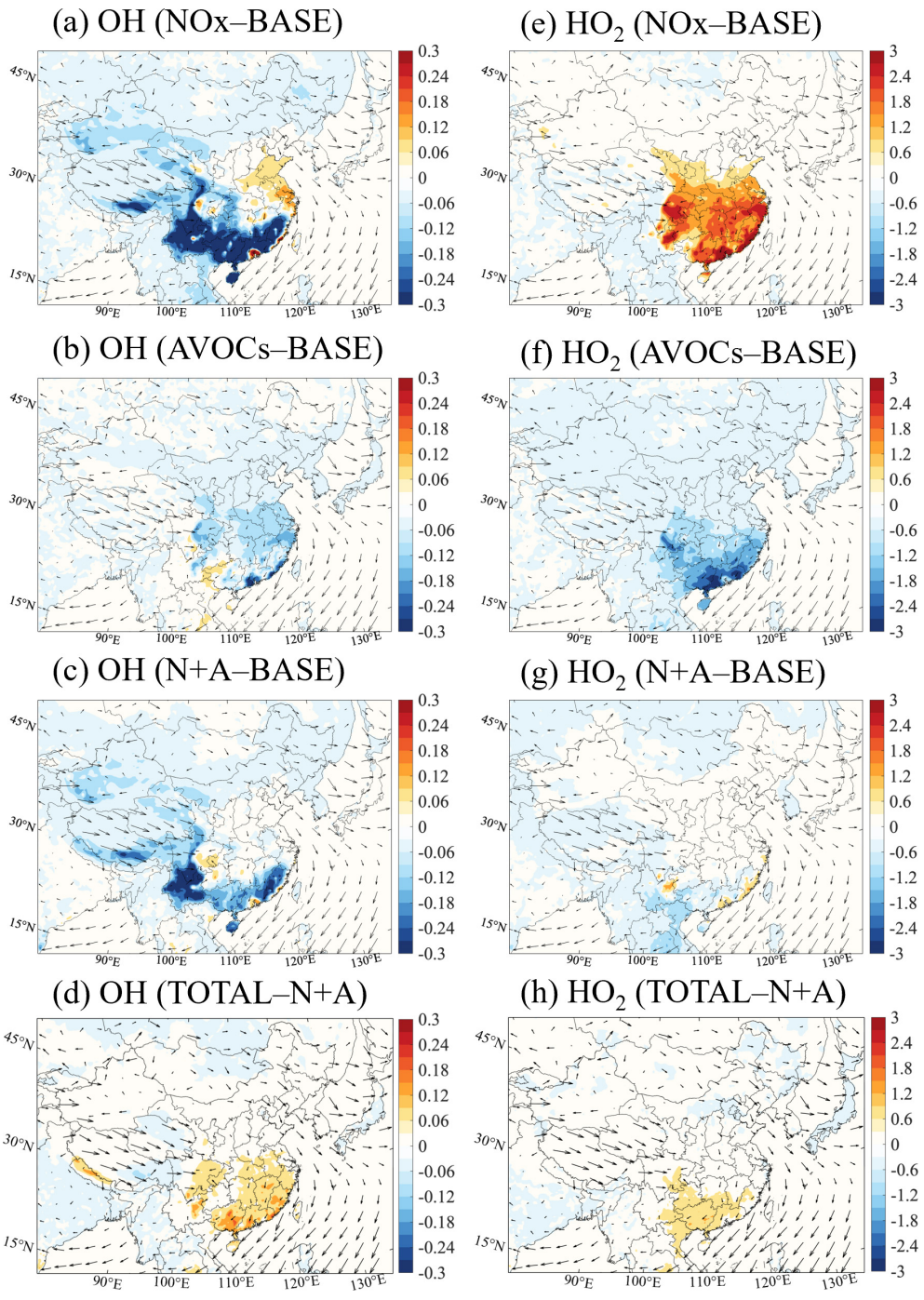

Figure 2. Changes in the monthly averaged daytime (06:00 to 19:00 LST) surface mixing ratio of the OH radical (**a–d**, 0.1 pptv) and HO_2 radical (**e–h**, pptv) responses to a 50 % reduction in the emissions of NO_x (**a, e**; *NOx* case), anthropogenic VOCs (**b, f**; *AVOCs* case), and NO_x and AVOCs (**c, g**; $N + A$ case) relative to the *BASE* case, together with additional emission reduction in other species (**d, h**; *TOTAL* case) relative to the $N + A$ case of January 2018. The arrows represent the wind speed and wind direction.

reduced AVOC emissions. In the *AVOCs* case, the decreases in the radical levels and in the production rates of the radicals explain the wintertime ozone decreases derived in South China. Simultaneously, a slight increase in the mixing ratio of the OH radical is derived. This increase is related to the reduced extinction of solar radiation associated with the reduced aerosol load following the reduction in the AVOC emissions.

When the 50 % emission reduction in NO_x is combined with the 50 % reduction in AVOC emissions ($N + A$ case),

the distribution of changes in the OH radical is similar to the pattern induced by emission reduction in NO_x alone. However, a weakened increase is calculated, as the increase in the OH radical concentration with the reduced NO_x emissions is largely compensated for by the decrease in the radical concentrations produced by the reduction in the AVOC emissions. As shown in Fig. 2c, the maximum increase in the OH radical in urban China is reduced to 12 % (from 40 %). At the same time, the increases in the mixing ratios of the HO_2 radicals are reduced to 20 % (from 60 %; Fig. 2g), with only a mild increase distributed along the coast of South China. This compensating effect of the combined emission reduction on the radical levels is also reflected in the changes in the ozone concentrations, highlighting a link between the variations in the concentrations of photochemical radicals and in the formation rate of ozone.

When accounting for the additional reduction in the emissions of other anthropogenic species (NH_3, SO_2, and CO) (*TOTAL* case), the mixing ratio of the OH radical is positively modified relative to the results obtained in the combined case ($N + A$ case). As shown in Fig. 2d, the mixing ratio of the OH radical is enhanced by up to 22 % in the PRD and SCB regions. This increase is due to the reduced consumption of the OH radical by the reduced emissions and related concentrations of CO (Figs. S9a and S1d). For the HO_2 radicals, the additional reduction in the other emissions contributes to a larger mixing ratio, with a pronounced increase in South China (of up to 18 %; Fig. 2h). This increase in the HO_2 radical mixing ratio is due to the increased oxidation of the VOCs by the OH radical and the reduced aerosol uptake of HO_2 associated with the decrease in the aerosol load. The consistent increase between the OH and HO_2 radical levels and the ozone concentrations in South China reveals a positive relation between radical enhancement and ozone production.

Summer conditions. Figure 3 displays the spatial distribution of the changes in the daytime surface mixing ratios of the OH and HO_2 radicals due to the applied reduction in the emissions of NO_x, AVOCs, combined NO_x and AVOCs, and additional species for July 2018. When applying a 50 % reduction in the NO_x emissions, the mixing ratios of the OH radicals decrease in large parts of China, with the maximum decrease reaching 40 % (0.15 pptv; Fig. 3a). The decrease in the concentration of the OH radicals can also be explained by the reduced consumption of OH by the reaction with NO_2 due to the reduced emissions of nitrogen oxides. The geographical area in which the concentration of OH radicals is reduced covers a large fraction of China, including its northern provinces. This area is different from the wintertime situation, when the OH reduction only occurred in South China. The concentration of the OH radical increases in the metropolitan areas, including in the YRD and PRD regions. A consistent increase in the concentrations of the OH radicals is also found at the Shanghai and Guangzhou sites (Fig. S7). Simultaneously, the surface mixing ratio of the HO_2 radical increases by 15 %–20 % (6–8 pptv; Fig. 3e) in the North China Plain due to the reduced loss via aerosol uptake. The spatial shift in the distribution of radical changes from South China in winter to North China in summer is influenced by seasonal patterns of meteorological parameters, including temperature, water vapor abundance, and solar radiation intensity, which affect the atmospheric oxidative processes (Dai et al., 2023).

When AVOC emissions are reduced by 50 %, the mixing ratio of the radicals in urban areas, including in the NCP, YRD, and PRD regions, decreases on average by 8 %–12 % in the case of OH (0.03–0.05 pptv; Fig. 3b) and by 6 %–10 % in the case of HO_2 (3–5 pptv; Fig. 3f). When applying the combined 50 % emission reduction in AVOCs and NO_x, the changes in the patterns of the OH radical are similar to the distribution derived for the reduction in NO_x emissions alone, but this is also partially offset by the counteracting effect of AVOC emissions, as for winter conditions. As shown in Fig. 3c, the maximum increase in the OH radical is reduced to 20 % (from 40 %) and the maximum decrease is reduced to 12 % (from 30 %). The counteracting effect of AVOC emission reduction is also shown in the enhanced abundance of HO_2 radicals (Fig. 3g), with increases of less than 6 % (from 15 % to 20 %) in the urban areas.

With an additional 50 % reduction in other anthropogenic emissions, the changes in OH and HO_2 radicals relative to the results obtained in the combined case are smaller than the changes derived for winter conditions (Fig. 3d and h). This is due to the small decrease in the aerosol load during summer (see Sect. 3.2.3).

3.2.2 Changes in OVOCs

OVOCs originate from direct biogenic and anthropogenic surface emissions (primary source) and from the oxidation of primary hydrocarbons (secondary source) in the atmosphere (W. Wang et al., 2022). The photolysis of OVOCs produces photochemical radicals, which enter the formation of secondary pollutants and have a potential negative effect on ozone pollution mitigation.

Winter conditions. Figure 4 shows the spatial distribution of the calculated changes in the total OVOCs due to a 50 % reduction in the emissions of NO_x, AVOCs, combined NO_x and AVOCs, and additional species for January 2018. With the adopted reduction in NO_x emissions, the OVOC concentration decreases in the non-urban areas of South China and increases in urban China (Fig. 4a), which is consistent with the changes derived for the mixing ratio of the OH radical. The highest increase in the OVOC concentration is approximately 10 % (2 ppbv) in the urban areas of the YRD and PRD regions; this includes a significant increase in the concentration of HCHO (Fig. S10a), followed by peroxyacetyl nitrate (PAN; Fig. S10b) and alcohols (CH_3OH and C_2H_5OH; Fig. S10c), as the secondary formation of these OVOC species is determined by OH-related reactions (Em-

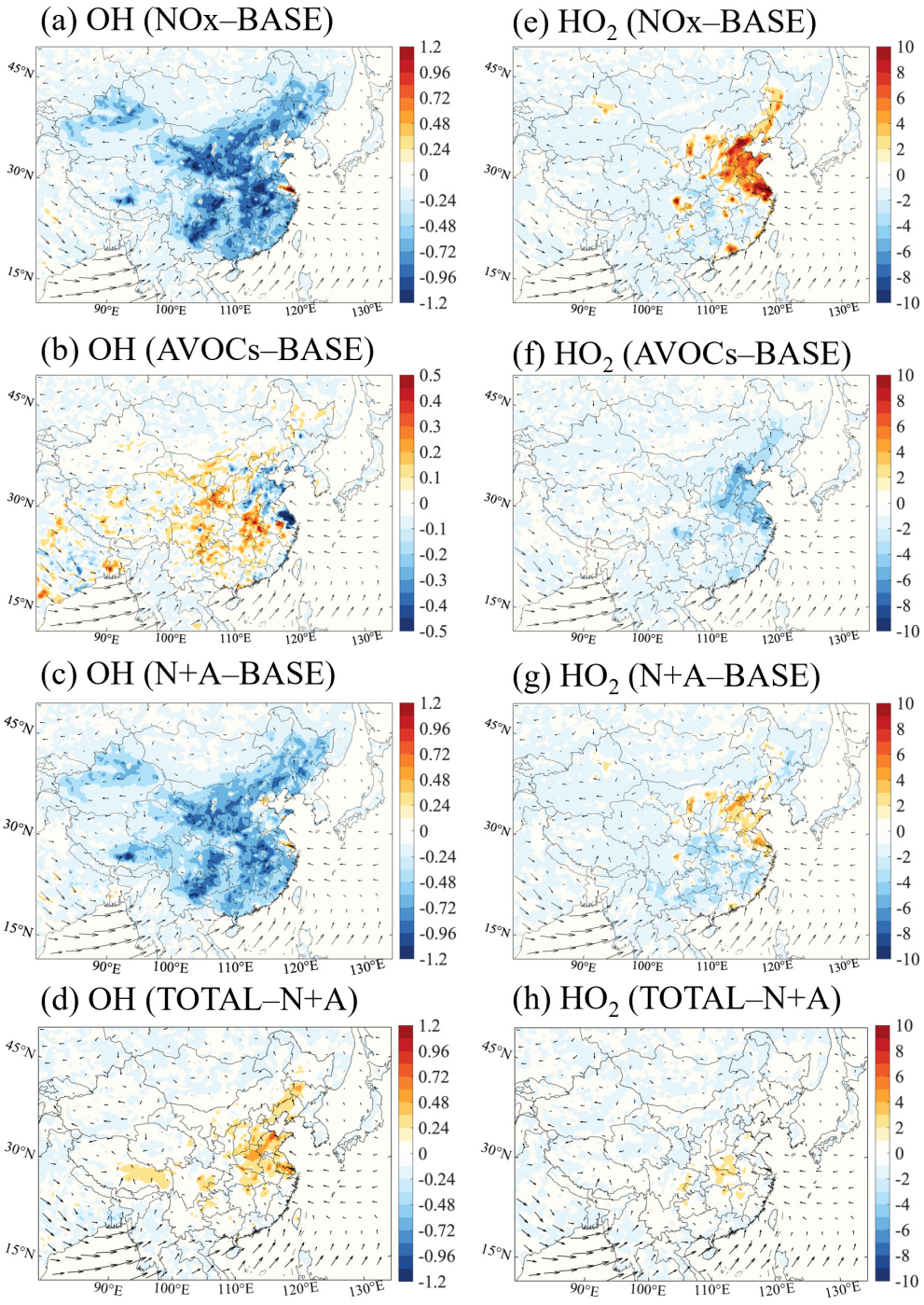

Figure 3. Same as Fig. 2 but for July 2018. Note the inconsistency in the scale of Fig. 2b.

mons et al., 2010). At the four city sites under consideration, the highest increase in OVOCs is found at Shanghai and Guangzhou, with concentrations increasing by about 12 % (1.8 ppbv; Fig. 4f) and 8 % (1.2 ppbv; Fig. 4g), respectively. This increase in the concentration of OVOCs is consistent with the higher increase in OH radicals at these two sites (Fig. S7).

When the AVOC emissions are reduced, the abundance of OVOCs is reduced in all the regions of China (Fig. 4b), with the highest decrease found in the PRD and SCB regions. At the four city sites under consideration (Fig. 4e–h), the decrease is most pronounced in the case of the concentration of ketones (see Table S2 for the specific OVOC speciation), including acetone (CH_3COCH_3), methyl

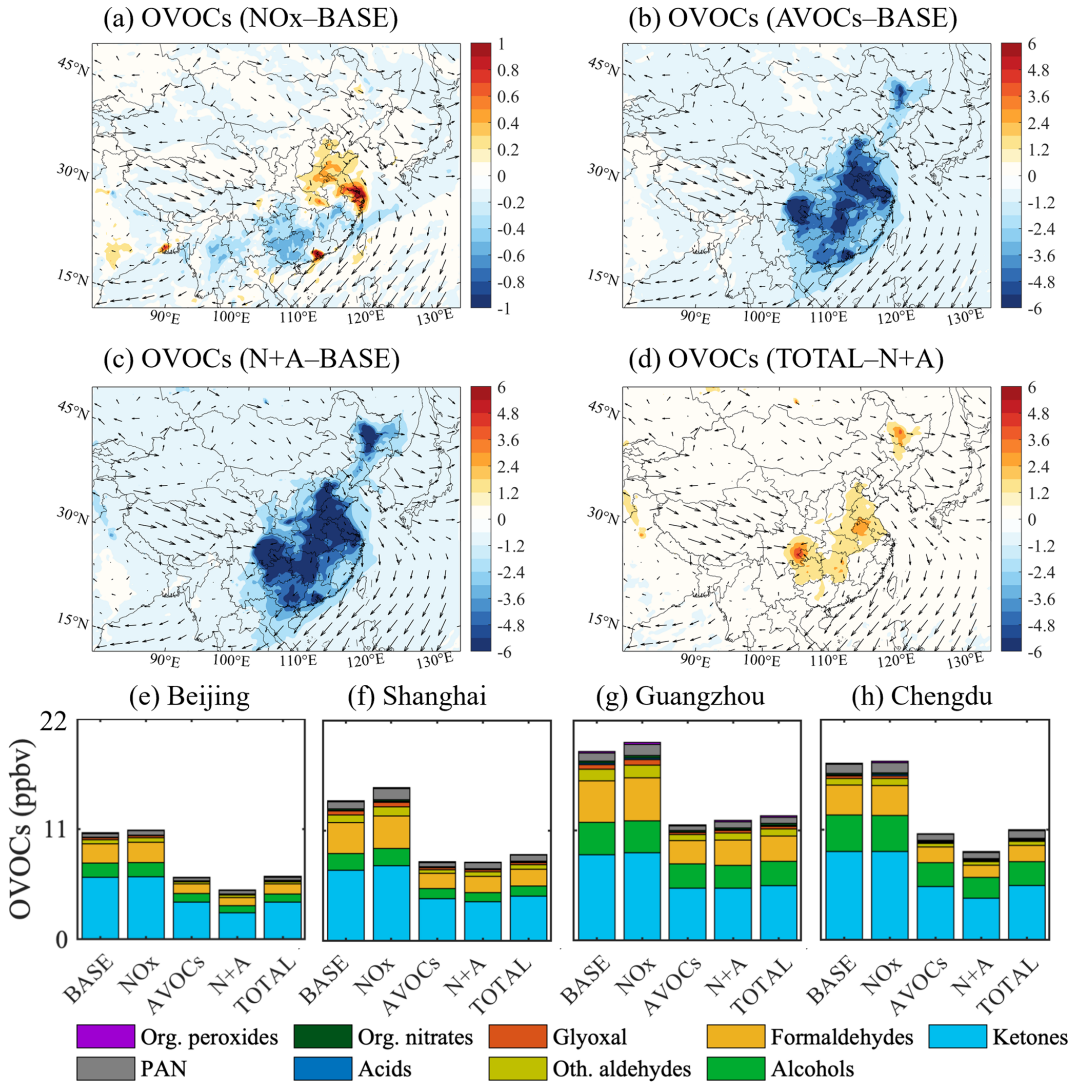

Figure 4. Changes in the monthly averaged surface concentration of total OVOCs for January 2018. **(a–d)** Changes in the concentration of the total OVOC (ppbv) response to the reduction in the emissions of NO_x (**a**, *NOx* case), anthropogenic VOCs (**b**, *AVOCs* case), and combined NO_x and AVOCs (**c**, $N + A$ case) relative to the *BASE* case, together with an additional emission reduction in other species (**d**, *TOTAL* case) relative to the $N + A$ case. **(e–h)** Averaged concentrations of OVOCs contributed by different species at four city sites (Beijing, Shanghai, Guangzhou, and Chengdu) in China in five simulated cases (*BASE*, *NOx*, *AVOCs*, $N + A$, and *TOTAL*). The arrows in panels **(a)**–**(d)** represent the wind speed and wind direction. Note the inconsistency in the scale of Fig. 3a.

vinyl ketone ($CH_3C(O)CHCH_2$), and methyl ethyl ketone ($CH_3CH_3C(O)CH_2CH_3$). The abundance of these species is reduced by nearly half, as the relevant ketones originate primarily from anthropogenic emissions. When combining the emission reduction in AVOCs and NO_x, the decrease in the OVOC concentration resulting from the AVOC emission reduction is further strengthened in large areas of China (Fig. 4c). With additional decreases in the other emissions, the OVOC concentration is enhanced by 2–4 ppbv in the whole of China (Fig. 4d), which is consistent with the increased abundance of the OH radical resulting from a reduction in the NH_3, SO_2, and CO emissions.

Summer conditions. Figure 5 displays the spatial distribution of the changes in total OVOC concentrations in response to a 50 % reduction in the emissions of NO_x, AVOCs, combined NO_x and AVOCs, and additional species for July 2018. With a 50 % reduction in NO_x emissions, a slight decrease in the OVOC concentrations (0.5–1.5 ppbv or 3 %–8 %) is derived in South China (Fig. 5a), which is predominantly contributed by the decreases in the concentrations of HCHO, glyoxal, and PAN (Fig. S11a–c). The decreases in these OVOC species are due to a lower contribution from the secondary formation from OH-related reactions, as a consistent decrease is calculated for the changes in the OH rad-

ical. However, in Central and North China, the calculated concentrations of OVOCs generally increase (0.5–2.0 ppbv or 5 %–8 %). This increase is mainly contributed by the enhancement in the concentration of aldehydes (Fig. S12a) and alcohols (Fig. S12b). The increase in OVOC species is possibly due to the enhanced contribution from the reactions between alkenes and isoprene, whose concentrations are increased (Fig. S12c, d), and enhanced oxidants. This result indicates that reducing anthropogenic emissions of aldehydes and alcohols may help offset the increase in OVOCs caused by the reduction in NO_x emissions.

With a 50 % reduction in AVOC emissions, the OVOC concentrations are significantly reduced in the NCP and SCB regions (by 20 %–30 % on average; Fig. 5b). Compared with the reduced OVOC concentration (by 50 %) in winter, the summertime response of OVOCs to the AVOC emission reduction is smaller. Consistently, at the Beijing site (Fig. 5e), the decrease in the OVOC concentration is calculated as 30 % (10 ppbv) on average, which is smaller than the decrease of 46 % (5 ppbv) in winter. This seasonal difference is attributable to the higher photochemical formation of OVOCs during summertime, which is favored by the higher levels of temperature, solar radiation, and temperature-dependent biogenic emissions. The smaller decrease in the alcohol concentration (from 1.5 ppbv in winter to 0.5 ppbv in summer; Fig. S13) also supports our finding, as its summertime formation is highly dependent on the photochemical reactions with BVOCs (Zhang et al., 2023). Considering the increases in aldehydes and alcohol levels induced by the reduced NO_x emission, this result also reveals a need to reduce the primary emissions of these two OVOCs to effectively control their negative impact on ozone pollution mitigation.

When the combined reduction in the emissions of AVOCs with NO_x is considered, a lower decrease (by 15 %–26 %; Fig. 5c) is found in the concentration of OVOCs in the geographical areas of China compared to the response derived for the individual reductions in the NO_x or AVOC emissions. This response is consistent with the relevant changes in levels of OH radicals. When the emission reduction is applied to the other species under consideration, the response of the OVOC concentration to the reduced emissions is small (< 2 ppbv or 5 %; Fig. 5d).

3.2.3 Changes in aerosol

Figure 6 shows the changes in the average concentrations of secondary aerosol resulting from a 50 % reduction in the emissions of NO_x, AVOCs, the combined NO_x, AVOCs, and additional species in January and July 2018.

Winter conditions. In January, the 50 % reduction applied to NO_x leads to a large decrease in the aerosol load (10–18 $\mu g\,m^{-3}$ or 12 %–20 %; Fig. 6a) in Central and South China. The aerosol decrease predominantly results from the decrease in the NO_3^- abundance (Fig. S14a) linked to the reduced concentration of NO_2, followed by the reduction in the concentration of NH_4^+ (Fig. S14b). A slight increase in the abundance of secondary organic aerosols (SOA) is derived in the urban areas of the NCP, YRD, and PRD regions (1–2 $\mu g\,m^{-3}$ or 3 %–5 %; Fig. S14c), which is consistent with the increase in the level of oxidants, including the ozone and OH radicals. With a 50 % reduction applied to AVOC emissions, the changes in the aerosol concentration are smaller than with the 50 % reduction applied to the NO_x emissions. The corresponding aerosol decrease of less than 4 % (5 $\mu g\,m^{-3}$; Fig. 6b) predominantly results from the reduction in SOA concentrations (Fig. S15a). With a joint reduction in the emissions of NO_x and AVOCs (Fig. 6c), the decrease in the aerosol burden is larger than from the separated decrease in the individual emissions; this is explained by the fact that the increase in the concentration of SOA resulting from the reduced NO_x emissions is compensated for by the reduced AVOC emissions.

With a further reduction applied to the other emissions (*TOTAL* case), the decrease in the aerosol concentration is greatly enhanced in South China (Fig. 6d). This results in large part from the decrease in NO_3^- particles (by 5 $\mu g\,m^{-3}$; Fig. S16c), followed by the decreases in the concentrations of NH_4^+ (by 2 $\mu g\,m^{-3}$; Fig. S16a) and SO_4^{2-} (by 1 $\mu g\,m^{-3}$; Fig. S16b). The decreases in the NH_4^+ and SO_4^{2-} concentrations are due to the reduction in the concentrations of their gas-phase precursors NH_3 and SO_2. The decrease in the abundance of NO_3^- results from the formation of ammonium nitrate (NH_4NO_3) through the reaction of NH_3 with HNO_3 (Meng et al., 2022). This decrease in the aerosol burden explains the enhancement of HO_2 radicals since the aerosol uptake is reduced. This, in turn, promotes an increase in the ozone concentration in South China. At the four city sites, the largest decrease in the aerosol concentration is found at the Beijing site (Fig. S17), followed by the Chengdu site. This is attributed to the relatively high aerosol levels at these two locations. In our model, the concentrations of NO_2 and $PM_{2.5}$ are overestimated for the baseline conditions (Dai et al., 2023), which can possibly lead to an excessively high reduction in the aerosol concentration, especially in the concentration of NO_3^-. This overestimation potentially affects the aerosol-related changes in the ozone formation.

Summer conditions. In July, the decrease in the aerosol load due to the emission reduction is much smaller than in winter. The reductions range from 1.5 to 5 $\mu g\,m^{-3}$ (Fig. 6e), from 2 to 6 $\mu g\,m^{-3}$ (Fig. 6f), from 4 to 7 $\mu g\,m^{-3}$ (Fig. 6g), and from 8 to 10 $\mu g\,m^{-3}$ (Fig. 6h) for the reductions in the *NOx*, *AVOCs*, *N + A*, and *TOTAL* emission conditions. As for ozone, the reduction in aerosols also undergoes a spatial shift from South China in winter to North China in summer. This shift is consistent with the calculated changes in oxidants, hydrocarbons, and other gaseous aerosol precursors. The higher decrease in the aerosol load for the combined case also indicates that the reduction in AVOC emission increases the effi-

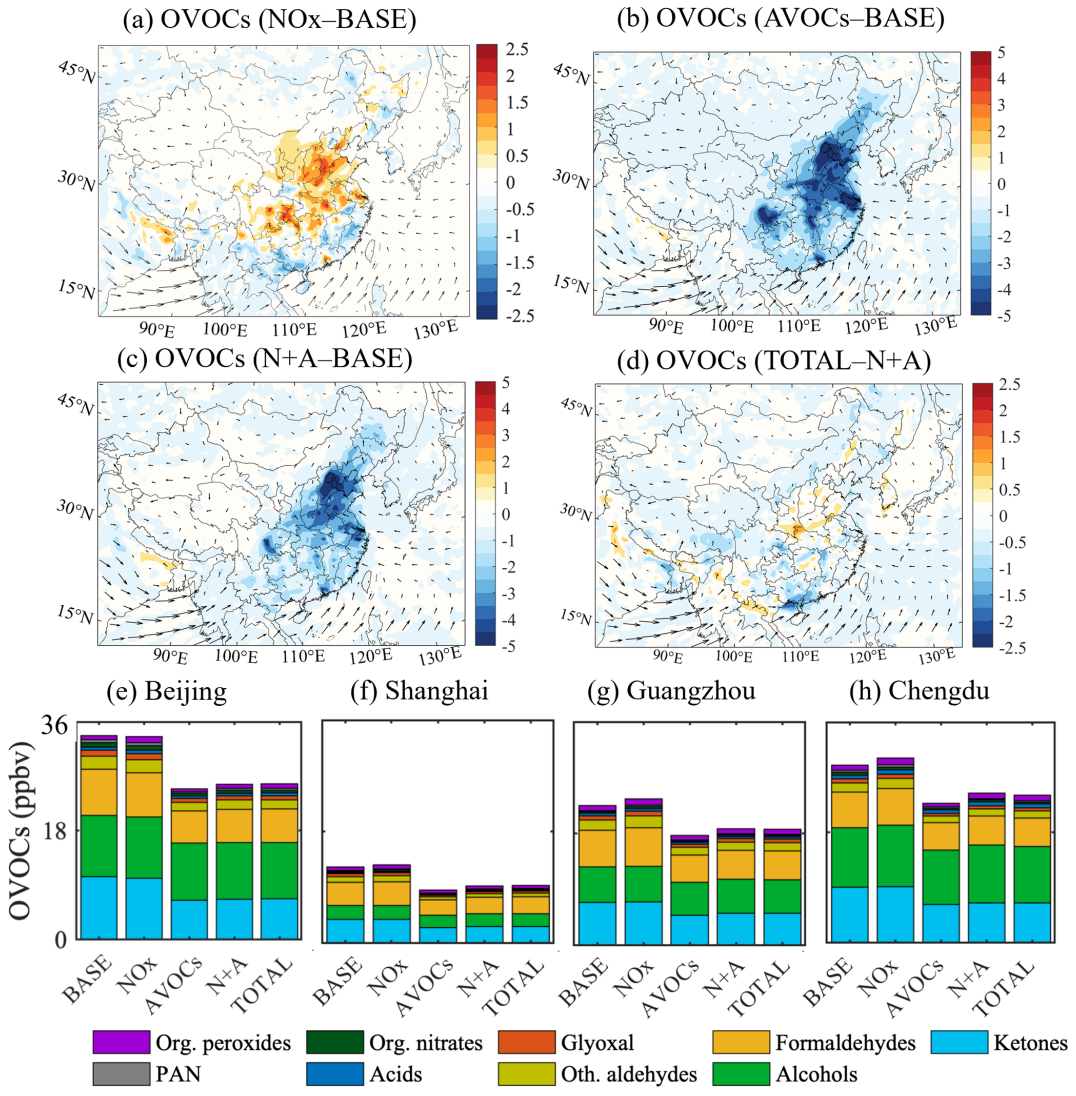

Figure 5. Same as Fig. 4 but for July 2018. Note the inconsistency in the scale of the figure.

ciency of the aerosol decrease produced by the reduced NO_x emissions.

The aerosol effect on ozone formation has been discussed in several modeling studies (Li et al., 2019; Liu and Wang, 2020; Dai et al., 2023). Our results show that the reduction in primary emissions results in a large decrease in aerosol concentrations. The major contribution to the aerosol decreases results from the reduction in NO_x emissions, with a strengthened effect when combined with a reduction in the AVOC emissions. This decrease in the aerosol burden weakens the aerosol extinction effect and therefore enhances the photochemical formation rate of radicals and ozone. As shown in Fig. S18a–d, the photolysis rate increases (by 5 %–20 %) in Central and South China during winter due to the aerosol decrease induced by the emission reductions. The highest increase in the photolysis rates results from the joint emission reduction in NO_x and AVOCs (Fig. S18c). The increase in the photolysis rates in summer is not as distinct as the increase during winter due to the limited reduction in the aerosol burden during summer (Fig. S18e–h).

Further, the reduction in the aerosol burden lowers the aerosol uptake of NO_2 and HO_2 radicals, which indirectly enhances the mixing ratio of OH and HO_2 radicals (Dai et al., 2023). An increased level of HO_2 radical following the emission reduction is caused by the reduced aerosol uptake. Large uncertainties still exist in the adopted value of the uptake coefficient of HO_2 (considered to be 0.1 in this study) (Yang et al., 2023). This affects the quantitative evaluation of the aerosol effects on the ozone levels and deserves further study. Considering the impact of aerosol load on ozone formation, it is essential to account for the aerosol effect on ozone formation, even with stringent emission reductions in the future.

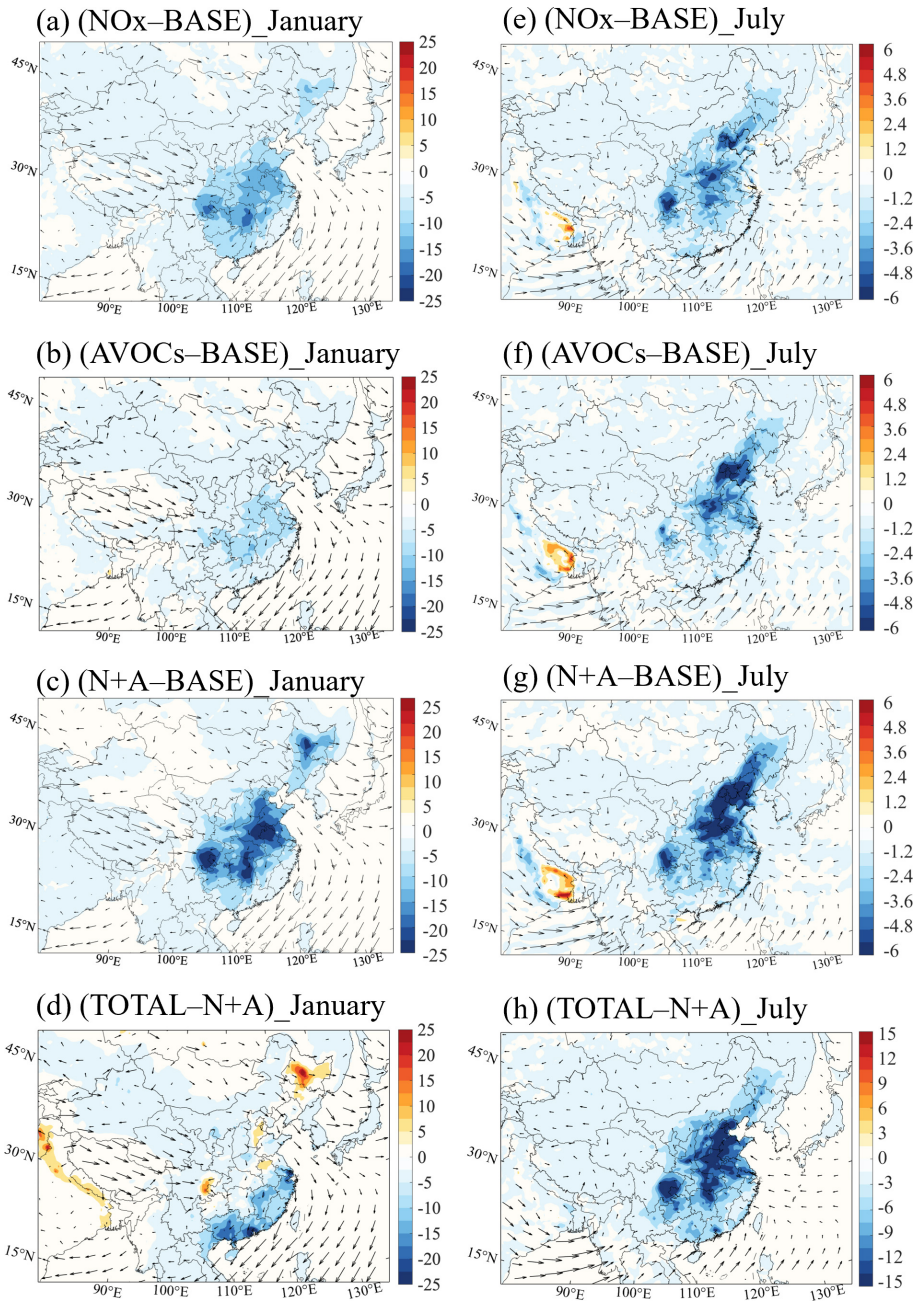

Figure 6. Changes in the monthly averaged surface concentration of fine particulate aerosol ($\mu g\,m^{-3}$) in response to the *NOx* **(a, e)**, *AVOCs* **(b, f)**, and $N + A$ **(c, g)** cases relative to the *BASE* case, the *TOTAL* case **(d, h)**, and the $N + A$ case for January **(a–d)** and July **(e–h)** 2018. The arrows represent the wind speed and wind direction. Note the inconsistency in the scale of panel **(h)**.

3.3 Response of ozone sensitivity regimes to emission reduction

Figure 7 displays the spatial distribution of ozone regimes in response to applied emission reductions for NO_x, AVOCs, combined NO_x and AVOCs ($N + A$), and additional species (*TOTAL*) in January and July.

Winter conditions. In January, when a 50 % reduction is applied to the NO_x emissions, the regions characterizing the ozone production in the south and southwest of China (*BASE* case; Fig. S2a) tend to be converted from transition or VOC-limited regimes to NO_x-limited areas (from 68.8 % in the *BASE* case to 71.9 % in the *NOx* case; Table S3) (Fig. 7a). The change in the ozone sensitivity regimes is consistent with (1) the reduced HNO_3 concentration (Fig. S19a) due to less NO_2 reacting with OH and (2) the enhanced H_2O_2 concentration (Fig. S10e) due to the reduced aerosol HO_2

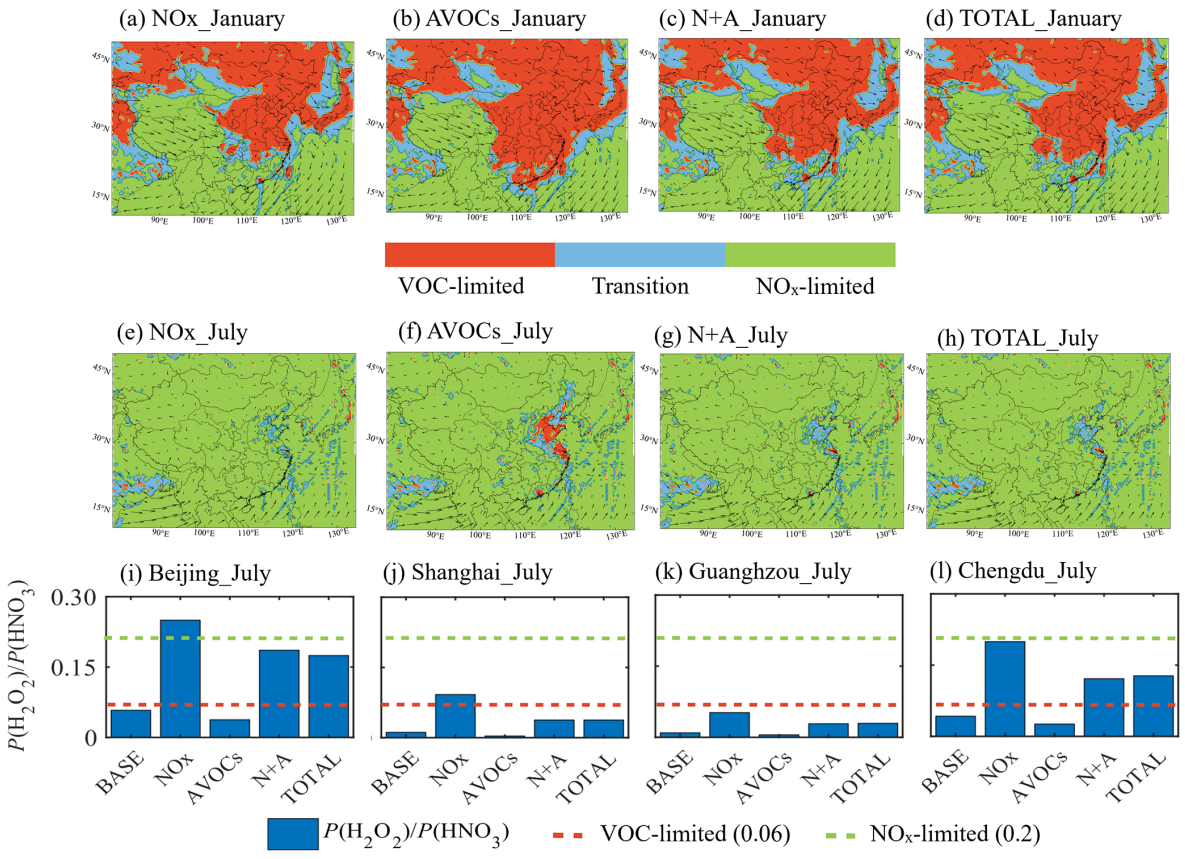

Figure 7. Impact of the emission reduction on ozone sensitivity regimes. **(a–h)** Display of ozone sensitivity regions in which ozone production is limited by the availability of nitrogen oxides (NO_x-limited, in green) and volatile organic compounds (VOC-limited, in red) under *NOx*, *AVOCs*, $N + A$, and *TOTAL* conditions in January **(a–d)** and July **(e–h)** 2018. The regions where ozone production is controlled by the availability of both NO_x and VOCs (transition) are shown in blue. **(i–l)** Averaged daytime (06:00 to 19:00 LST) values of the ratio between the production rate of hydrogen peroxide (H_2O_2) and nitric acid (HNO_3) [$P(H_2O_2)/P(HNO_3)$] at four city sites (Beijing, Shanghai, Chengdu, and Guangzhou) in the five simulated cases (*BASE*, *NOx*, *AVOCs*, $N + A$, and *TOTAL*) for July 2018.

uptake by aerosol particles. With a 50 % reduction applied to the AVOC emissions, some transition areas of South China are converted to VOC-limited areas (Fig. 7b; from 20.1 % in the *BASE* case to 21.3 % in the *AVOCs* case). A relevant decrease in the H_2O_2 concentration, derived in South China (Fig. S19f), is attributed to the decrease in the calculated HO_2 concentration. When considering the combined reduction in NO_x and AVOC emissions as well as the reduction in all anthropogenic emissions, the VOC-limited regions of South China evolve towards a transition region or even a NO_x-limited region (Fig. 7c, d). In these last two cases, the changes in ozone sensitivity regimes are determined by the decreases in the calculated HNO_3 concentrations (Fig. S19c, d). At the urban sites, the emission reduction does not modify the wintertime ozone sensitivity regimes (Fig. S20), which remain VOC-limited.

Summer conditions. In July, the changes in ozone regimes related to emission reductions are mainly found in VOC-limited areas and their surroundings, due to consistent changes in H_2O_2 and HNO_3 (Fig. S21). With the reduction in NO_x emissions, the size of VOC-limited areas shrinks and becomes a smaller fraction of the urbanized areas (Fig. 7e; from 3.4 % in the *BASE* case to 2.9 % in the *NOx* case). The regimes at three urban sites, which are VOC-limited in the *BASE* case, are modified: the ozone sensitivity at Beijing is converted to a NO_x-limited case (Fig. 7i), while the Shanghai (Fig. 7j) and Chengdu (Fig. 7l) sites are shifted towards a transition regime. The changes in ozone sensitivity at these three city sites result from the decreased production of HNO_3 due to reduced NO_2 and the increased production of H_2O_2 due to reduced HO_2 loss via aerosol uptake. The Guangzhou site remains in a VOC-limited region (Fig. 7k). Reasons for this exception could be the lower aerosol load (Fig. S17) and higher temperature-dependent BVOC emissions in the location (Dai et al., 2023), as its surroundings are covered by vegetation (Zhang et al., 2023).

With the reduction in AVOC emissions, the VOC-limited areas expand to the surroundings of the metropolitan areas (Fig. 7g; 3.7 % in the *AVOCs* case). Finally, when applying a combined 50 % reduction in the emissions of NO_x and

AVOCs ($N + A$ case; Fig. 7g) as well as a reduction in all other emitted species (*TOTAL* case; Fig. 7h), the patterns of the calculated change in the ozone sensitivity are similar to the patterns corresponding to the NO_x emissions; specifically, the VOC-limited area (3.0 % in the $N + A$ and *TOTAL* cases) becomes smaller relative to the *BASE* case. In these cases, the Beijing and Chengdu sites shift to a transition condition, while the Guangzhou and Shanghai sites remain under VOC-limited conditions. This result is consistent with the ozone increase obtained for the $N + A$ and *TOTAL* cases at the Guangzhou site.

3.4 Changes in the AOC

The AOC characterizes the self-cleansing ability of the atmosphere (Dai et al., 2023). This parameter is expressed as

$$\mathrm{AOC} = \sum_i^j k_{i,j}\,[Y_i]\left[X_j\right].$$

Here, $k_{i,j}$ represents the reaction rates between CO, methane (CH_4), and non-methane hydrocarbons (NMHCs) (denoted here as Y_i) and between the OH radical, the NO_3 radical, and O_3 (denoted here as X_j).

The changes in the spatial distribution of daytime (06:00 to 19:00 LST) AOC resulting from the adopted 50 % reduction in the emissions of ozone precursors for January and July 2018 are depicted in Fig. 8.

Winter conditions. In January, the 50 % reduction in NO_x emissions leads to a decrease in the daytime AOC of 10 %–20 % in South China and an increase of 10 %–18 % in the urban areas, including the PRD, YRD, and SCB regions (Fig. 8a). At the four city sites (Fig. 9a–d), the increase in the daytime AOC is attributed to the enhanced contributions of the OH-related reactions, including the reactions of OH with alkenes, followed by the reactions of OH with OVOCs and with aromatics. This daytime increase in AOC is consistent with the enhanced levels of the OH radicals, alkenes, and OVOCs when the NO_x emissions are reduced. The change in AOC with NO_x emission reduction allows us to characterize the formation process of O_3 and can be used as an indicator to design mitigation policies for reducing ozone pollution. During nighttime (20:00 to 05:00 LST), the reduction in NO_x emissions is responsible for an increase in AOC of up to 50 % (Fig. S22a). A contribution to this increase is provided by the alkenes' ozonolysis, since the concentrations of ozone (Fig. 6a) and alkenes (Fig. S12c) are enhanced. The largest increase in the alkene ozonolysis (from 31 % to 40 %; see Fig. S23b) is derived at the Shanghai site. These results highlight the enhanced oxidative processes associated with the NO_x emission reduction.

With the 50 % reduction in AVOC emissions, the daytime AOC is reduced in all the major regions of China (Fig. 8b), with the largest decreases occurring in the southern part of the country; specifically, the largest decrease occurs at the Guangzhou site (by 50 %). This decrease in daytime AOC is mainly attributable to the reduced contribution from the reactions between OH and alkenes, followed by the reactions of OH with aromatics and OVOCs. With a combined reduction in the emissions of NO_x and AVOCs ($N + A$; Fig. 8c), the distribution patterns of the changes in the daytime AOC are similar to the patterns found in the *AVOCs* case but are characterized by higher decreases in the daytime AOC. With the additional reduction in the other emissions considered here (*TOTAL*; Fig. 8d), an increase (relative to the *BASE* case) in the daytime AOC is derived in Central and South China; this result is consistent with the increase in OH radical levels and ozone concentrations.

Summer conditions. During summertime, the decrease in the daytime AOC is more pronounced than during wintertime. With the 50 % reduction applied to NO_x emissions, the daytime AOC decreases in large areas of China (ranging from 10 % to 20 %; Fig. 8e), while, in urban areas, an increase is predicted, including at the Guangzhou (8 %; Fig. 9g), Shanghai (5 %; Fig. 9f), and Chengdu (3 %; Fig. 9h) sites. However, at the Beijing site, the daytime value of the AOC decreases (Fig. 9e) because of the shift in the ozone sensitivity regime (from VOC-limited to NO_x-limited conditions). During nighttime, the NO_x emission reduction also leads to an increase in the AOC due to the alkene ozonolysis (Fig. S22b), with the largest increase derived at the Beijing site (from 10 % to 14 %; Fig. S23e).

With other emission reduction cases (*AVOCs* and $N + A$; Fig. 8f, g), the daytime AOC decreases in the whole of China, with more distinct decreases (relative to winter conditions) occurring in North China. With the reduction in the AVOC emissions, the relative decrease in daytime AOC is smaller than in winter, especially at the Guangzhou site (to 30 %), indicating a more important secondary formation of VOC-related AOC during summer. When the emissions of NO_x and AVOCs are jointly reduced by 50 %, the role of the reaction between OH and BVOCs in the determination of AOC is enhanced at the four city sites, with the largest increase (15 %) found at the Guangzhou site. This increase results from the enhanced levels of OH radicals (Fig. 2c) and in the presence of BVOC species, such as isoprene (Fig. S24).

The distribution patterns of changes in the daytime AOC due to emission reduction are largely consistent with the changes in the mixing ratio of the OH radicals and the changes in the concentrations of OVOCs, ozone, and SOA in both winter and summer. These consistent patterns suggest that the AOC is an appropriate indicator for characterizing the changes in secondary pollutants attributed to emission reduction. One exception is found when considering the changes in the ozone concentration resulting from the reduction in NO_x emissions during winter. During this season, a comparison between the values of the daytime AOC and the changes in the ozone concentration (Fig. 5a) suggests that the change in the daytime AOC primarily reflects the changes in the net production rate of odd oxygen (Fig. S25); this can be

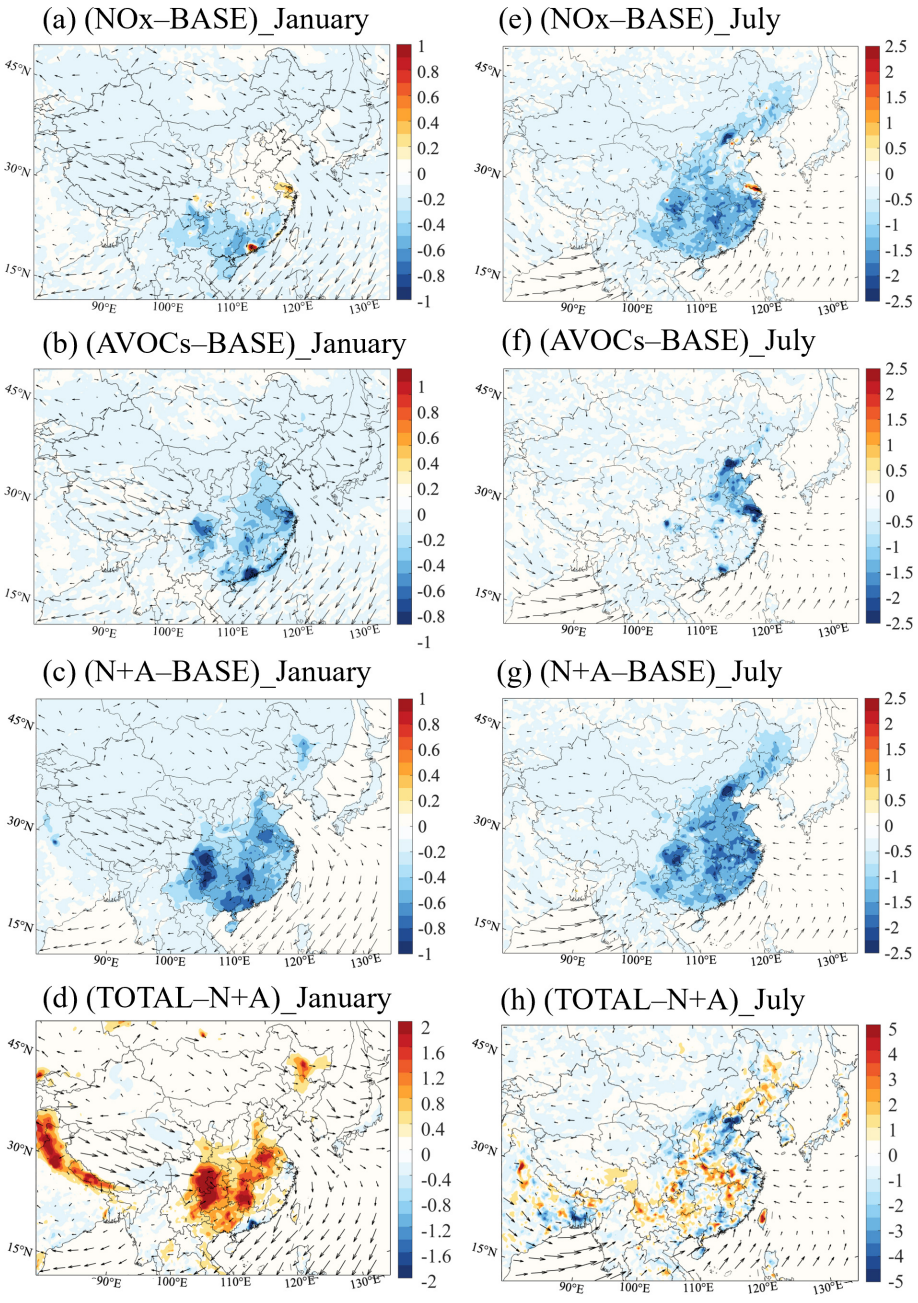

Figure 8. Changes in the monthly averaged daytime value of the AOC response to the NO_x **(a, e)**, *AVOCs* **(b, f)**, and $N + A$ **(c, g)** cases relative to the *BASE* case (10^7 molec. cm^{-3} s^{-1}) and the response to the *TOTAL* case **(d, h)** relative to the $N + A$ case (10^6 molec. cm^{-3} s^{-1}) for January **(a–d)** and July **(e–h)** 2018.

explained by the important role played by NO_2 in the wintertime formation of ozone.

4 Summary and policy implications

The model simulations performed in the present study explore the responses of radicals, ozone, and the atmospheric oxidative processes to a 50 % reduction applied to the primary emissions of key pollutants. Our analysis provides insight into the changes affecting ozone chemistry and the oxidizing processes to be expected in response to future emission reduction.

In winter, as most geographical areas are VOC-limited (saturated in NO_x), a 50 % reduction in NO_x emissions leads to an ozone concentration increase of up to 8–10 ppbv (15 %–25 %) in all the geographical regions of China; this increase results from the reduced titration of ozone by nitric oxide.

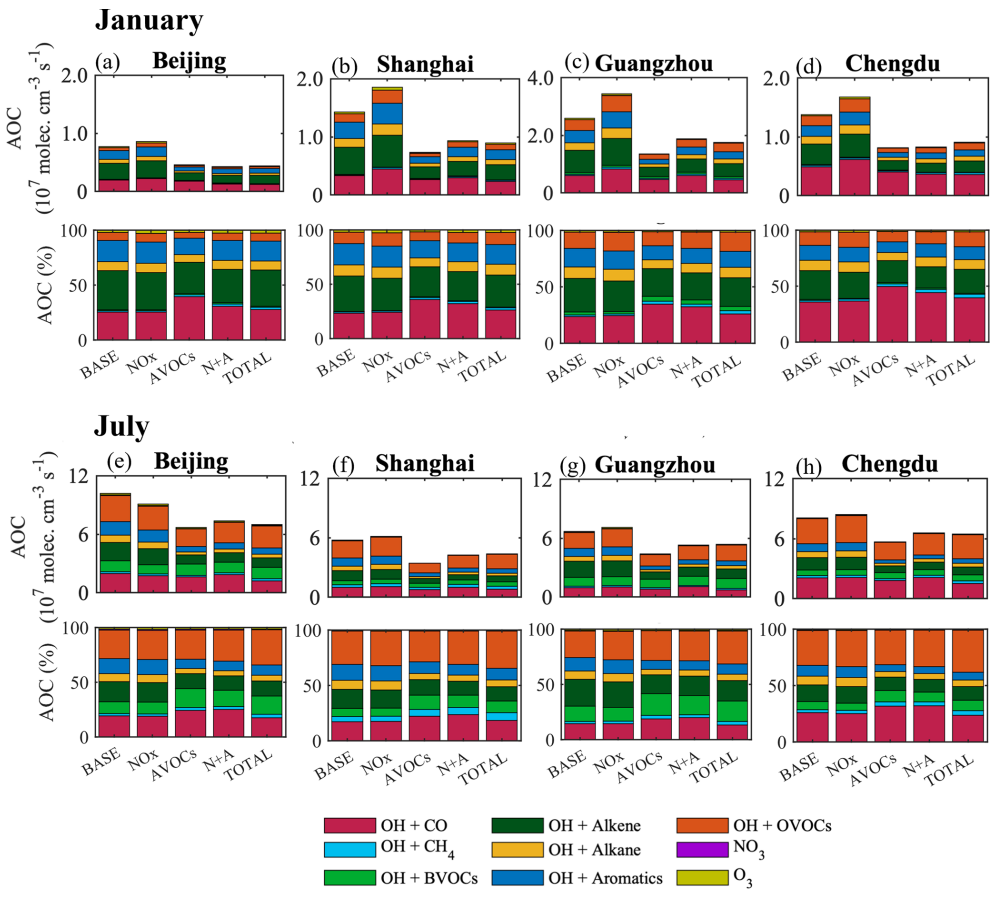

Figure 9. Monthly averaged value (10^7 molec. cm^{-3} s^{-1}) and relative terms (%) of the daytime AOC values at the Beijing **(a, e)**, Shanghai **(b, f)**, Guangzhou **(c, g)**, and Chengdu **(d, h)** sites in five simulated cases (*BASE*, *NOx*, *AVOCs*, $N + A$, and *TOTAL*) in January **(a–d)** and July **(e–h)** 2018. Note the inconsistency in the scale of panel **(c)**.

When combining this NO_x reduction with a 50 % reduction applied to AVOC emissions, the ozone enhancement found in the rural areas and resulting from the reduced NO_x is considerably lower. However, in urban areas (VOC-limited situation), the ozone increase, although weakened, still exists (by 3.0–7.5 ppbv).

In summer, as most rural areas of China become NO_x-limited, the geographical regions covered by the ozone increase in response to the 50 % reduction applied to the NO_x emissions shrink almost to the sizes of the VOC-limited metropolitan areas. In these urban environments, the ozone increase reaches a maximum of 10 ppbv or 17 %. When the NO_x emission reduction is combined with a 50 % reduction in the VOC emissions, the increase in ozone almost disappears in all areas of China. This is explained by the significant decrease in the ozone production resulting from the reduced levels of hydrocarbons. However, in the areas where hydrocarbons are primarily of biological origin, the ozone concentration (i.e., linked to the photochemical degradation of isoprene) still increases slightly (i.e., by 0.5 ppbv or 1.3 % at the Guangzhou site).

Paths to mitigation. We conclude this paper by highlighting a few chemical paths that should be considered when designing mitigation policies for the reduction of ozone in urban areas of China. Figure 10 presents a schematic description of the chemical mechanisms involved in the chemical production of atmospheric ozone and highlights how different reaction paths tend to change the ozone abundance in response to a reduction in NO_x and AVOC emissions. This figure shows that a reduction in NO_x emissions tends to increase the ozone concentration by (1) reducing the rate of the $NO + O_3$ reaction (ozone titration), (2) increasing the rate of the $HO_2 + NO$ reaction due to an increase in the HO_2 level associated with the reduced uptake of this radical by a lowered aerosol load, and (3) increasing the AOC through OH-related reactions. The graph also shows that a decrease in AVOC emissions tends (1) to reduce the level of the HO_x radical and hence the ozone production by the $HO_2 + NO$ reaction, (2) to enhance the level of OH radicals due to the reduced aerosol uptake, and (3) to reduce the AOC with a negative change in the ozone concentration. The relative im-

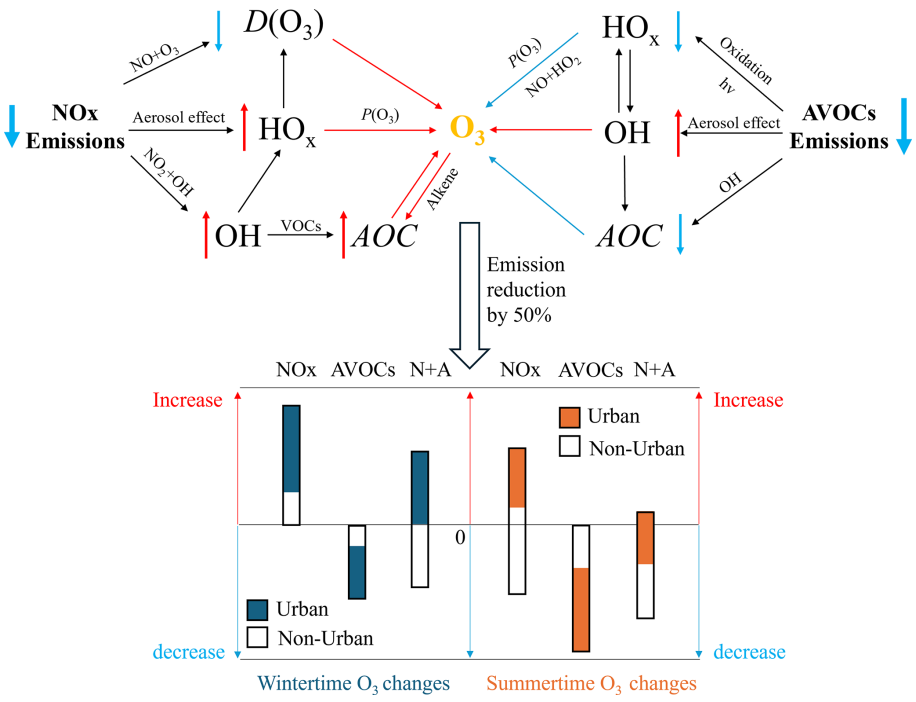

Figure 10. The schematics show the responses of oxidative processes, associated with ozone formation, to the reduction in primary emissions of NO_x and AVOCs in urban areas (VOC-limited) in winter and summer. The arrows next to the chemicals represent the changes associated with the reduction in emissions (decreasing trend shown in blue; increasing trend shown in red). The blue and red arrows close to O_3 represent the positive and negative contributions to the ozone formations. AOC, $P(O_3)$, and $D(O_3)$ are the abbreviations of the atmospheric oxidative capacity, production of ozone, and destruction of ozone. The bar figure shows the ranges of ozone changes in the whole of China (black bar), in non-urban areas (white part of the bar), and in urban areas (colored part of the bar) in three emission cases (*NOx*, *AVOCs*, and $N + A$ represent the cases with emission reductions in NO_x, AVOCs, and the combined NO_x and AVOC emissions, respectively) relative to the *BASE* cases under winter and summer conditions.

portance of these different chemical mechanisms varies with the location and the environmental conditions.

We conclude that, *in winter*, when the background ozone concentration is low, the reduction in NO_x emissions tends to increase the level of near-surface ozone, while the reduction in AVOC emissions has the opposite effect. This conclusion applies to both rural and urban areas. A combined reduction in the emissions of these two primary pollutants tends to decrease the level of ozone in rural areas but increase ozone in urban areas. Thus, in urban areas during winter, an effective approach to reducing the surface ozone concentration is a strong limitation of the emissions of volatile organic compounds.

In summer, when the ozone level is generally high, the reduction in NO_x emissions is an effective action to reduce the ozone concentration in rural areas. This measure, however, is counterproductive in the NO_x-saturated urban areas, where ozone is controlled by VOCs. In fact, in urban areas during this season, the mechanisms involved in ozone mitigation are complex. For example, when NO_x emissions are reduced, the atmospheric OH concentration is enhanced because of its reduced destruction by NO_2. Following this increase in the OH concentration, an increase in the levels of OVOCs, whose photolysis is an important source of HO_x radicals, also leads to accelerated ozone production and further amplifies the oxidation of VOCs. In addition, the increase in AOC, linked to the reactions of OH and ozone with alkenes and the reactions of OH with OVOCs, contributes to an increase in the ozone production. Further, the reduction in the aerosol load, resulting from a reduction in the emissions of aerosol precursors, promotes ozone formation by decreasing the aerosol extinction of light and reducing the uptake of HO_2. When combined with a 50 % reduction in AVOCs, the increase in the OVOC concentrations and AOC, resulting from reduced NO_x emissions, can be offset. However, the aerosol-related promotion of the levels of OH and HO_2 radicals can be enhanced, highlighting the complexity of summertime ozone mitigation in urban areas.

Overall, in urban areas, the reduction in the surface ozone levels requires a reduction in the emissions of anthropogenic VOCs. These results are consistent with the studies of Wang et al. (2023) and Liu et al. (2023), who stated that the aim of ozone pollution control in China should be to reduce the emissions of VOCs. Our study assumes a uniform 50 % reduction in the emissions of all primary VOCs. Future work should therefore determine which of these VOCs should be

reduced as a priority to determine the most effective ozone control strategy. Our results suggest that reducing emissions of alkenes, aromatics, and unsaturated VOCs, especially methanol and ethanol, should be a priority. To develop efficient mitigation strategies that reduce anthropogenic VOC emissions, more detailed investigations are needed into the reactivity of individual VOCs and their potential impact on urban ozone formation.

Code and data availability. The source code of WRF-Chem used in this work is available at https://github.com/wrf-model/WRF (last access: 7 March 2024, https://doi.org/10.5065/1DFH-6P97, Skamarock et al., 2019). The modified code in the WRF-Chem model is available upon request to the corresponding author. The air quality data at the surface stations are publicly available from the website of the Ministry of Ecology and Environment of the People's Republic of China at http://english.mee.gov.cn/ (last access: 14 April 2023, https://doi.org/10.5194/acp-23-14127-2023, Dai et al., 2023).

Supplement. The supplement related to this article is available online at: https://doi.org/10.5194/acp-24-12943-2024-supplement.

Author contributions. JD and GPB designed the structure of the manuscript, performed the numerical experiments, analyzed the results, and wrote the manuscript. JD analyzed the data and created the figures. All the co-authors provided comments and reviewed the manuscript.

Competing interests. At least one of the (co-)authors is a member of the editorial board of *Atmospheric Chemistry and Physics*. The peer-review process was guided by an independent editor, and the authors also have no other competing interests to declare.

Disclaimer. Publisher's note: Copernicus Publications remains neutral with regard to jurisdictional claims made in the text, published maps, institutional affiliations, or any other geographical representation in this paper. While Copernicus Publications makes every effort to include appropriate place names, the final responsibility lies with the authors. Regarding the maps used in this paper, please note that Figs. 1–6 and 8 contain disputed territories.

Acknowledgements. The National Center for Atmospheric Research (NCAR) is sponsored by the US National Science Foundation. We would like to acknowledge the high-performance computing support from NCAR Cheyenne.

Financial support. This research has been supported by the Deutsche Forschungsgemeinschaft, the National Natural Science Foundation of China (Air-Changes, grant no. 4487-20203), the Research Grants Council – University Grants Committee (grant no. T24-504/17-N), and the National Natural Science Foundation of China (grant no. 42293322).

The article processing charges for this open-access publication were covered by the Max Planck Society.

Review statement. This paper was edited by Benjamin A Nault and reviewed by two anonymous referees.

References

China Air: Air Pollution Prevention and Control Progress in Chinese Cities, http://www.allaboutair.cn/uploads/231027/ChinaAir2023EN.pdf (last access: 7 March 2024), 2023.

Dai, J., Brasseur, G. P., Vrekoussis, M., Kanakidou, M., Qu, K., Zhang, Y., Zhang, H., and Wang, T.: The atmospheric oxidizing capacity in China – Part 1: Roles of different photochemical processes, Atmos. Chem. Phys., 23, 14127–14158, https://doi.org/10.5194/acp-23-14127-2023, 2023.

Emmons, L. K., Walters, S., Hess, P. G., Lamarque, J.-F., Pfister, G. G., Fillmore, D., Granier, C., Guenther, A., Kinnison, D., Laepple, T., Orlando, J., Tie, X., Tyndall, G., Wiedinmyer, C., Baughcum, S. L., and Kloster, S.: Description and evaluation of the Model for Ozone and Related chemical Tracers, version 4 (MOZART-4), Geosci. Model Dev., 3, 43–67, https://doi.org/10.5194/gmd-3-43-2010, 2010.

Jacob, D. J., Horowitz, L. W., Munger, J. W., Heikes, B. G., Dickerson, R. R., Artz, R. S., and Keene, W. C.: Seasonal transition from NO_{x-} to hydrocarbon-limited conditions for ozone production over the eastern United States in September, J. Geophys. Res.-Atmos., 100, 9315–9324, https://doi.org/10.1029/94JD03125, 1995.

Knote, C., Hodzic, A., Jimenez, J. L., Volkamer, R., Orlando, J. J., Baidar, S., Brioude, J., Fast, J., Gentner, D. R., Goldstein, A. H., Hayes, P. L., Knighton, W. B., Oetjen, H., Setyan, A., Stark, H., Thalman, R., Tyndall, G., Washenfelder, R., Waxman, E., and Zhang, Q.: Simulation of semi-explicit mechanisms of SOA formation from glyoxal in aerosol in a 3-D model, Atmos. Chem. Phys., 14, 6213–6239, https://doi.org/10.5194/acp-14-6213-2014, 2014.

Li, B., Ho, S. S. H., Li, X., Guo, L., Chen, A., Hu, L., Yang, Y., Chen, D., Lin, A., and Fang, X.: A comprehensive review on anthropogenic volatile organic compounds (VOCs) emission estimates in China: comparison and outlook, Environ. Int., 156, 106710, https://doi.org/10.1016/j.envint.2021.106710, 2021.

Li, C., Liu, Y., Cheng, B., Zhang, Y., Liu, X., Qu, Y., and Feng, M.: A comprehensive investigation on volatile organic compounds (VOCs) in 2018 in Beijing, China: Characteristics, sources and behaviors in response to O_3 formation, Sci. Total Environ., 806, 150247, https://doi.org/10.1016/j.scitotenv.2021.150247, 2022.

Li, J., Xie, X., Li, L., Wang, X., Wang, H., Jing, S. A., and Hu, J.: Fate of Oxygenated Volatile Organic Compounds in the Yangtze River Delta Region: Source Contributions and Impacts on the Atmospheric Oxidation Capacity, Environ. Sci., Technol., 56, 11212–11224, 11212-11224.https://doi.org/10.1021/acs.est.2c00038, 2022.

Li, K., Jacob, D. J., Liao, H., Shen, L., Zhang, Q., and Bates, K. H.: Anthropogenic drivers of 2013−2017 trends in summer surface ozone in China, P. Natl. Acad. Sci. USA, 116, 422–427, https://doi.org/10.1073/pnas.1812168116, 2019.

Li, K., Jacob, D. J., Liao, H., Qiu, Y., Shen, L., Zhai, S., and Kuk, S. K.: Ozone pollution in the North China Plain spreading into the late-winter haze season, P. Natl. Acad. Sci. USA, 118, e2015797118, https://doi.org/10.1073/pnas.2015797118, 2021.

Liu, T., Hong, Y., Li, M., Xu, L., Chen, J., Bian, Y., Yang, C., Dan, Y., Zhang, Y., Xue, L., Zhao, M., Huang, Z., and Wang, H.: Atmospheric oxidation capacity and ozone pollution mechanism in a coastal city of southeastern China: analysis of a typical photochemical episode by an observation-based model, Atmos. Chem. Phys., 22, 2173–2190, https://doi.org/10.5194/acp-22-2173-2022, 2022.

Liu, Y. and Wang, T.: Worsening urban ozone pollution in China from 2013 to 2017 – Part 2: The effects of emission changes and implications for multi-pollutant control, Atmos. Chem. Phys., 20, 6323–6337, https://doi.org/10.5194/acp-20-6323-2020, 2020.

Liu, Y., Geng, G., Cheng, J., Liu, Y., Xiao, Q., Liu, L., and Zhang, Q.: Drivers of Increasing Ozone during the Two Phases of Clean Air Actions in China 2013–2020, Environ. Sci. Technol., 57, 8954–8964, https://doi.org/10.1021/acs.est.3c00054, 2023.

Meng, F., Zhang, Y., Kang, J., Heal, M. R., Reis, S., Wang, M., Liu, L., Wang, K., Yu, S., Li, P., Wei, J., Hou, Y., Zhang, Y., Liu, X., Cui, Z., Xu, W., and Zhang, F.: Trends in secondary inorganic aerosol pollution in China and its responses to emission controls of precursors in wintertime, Atmos. Chem. Phys., 22, 6291–6308, https://doi.org/10.5194/acp-22-6291-2022, 2022.

Ou, J., Yuan, Z., Zheng, J., Huang, Z., Shao, M., Li, Z., and Louie, P. K.: Ambient ozone control in a photochemically active region: short-term despiking or long-term attainment?, Environ. Sci. Technol., 50, 5720–5728, https://doi.org/10.1021/acs.est.6b00345, 2016.

Skamarock, W. C., Klemp, J. B., Dudhia, J., Gill, D. O., Liu, Z., Berner, J., Wang, W., Powers, J. G., Duda, M. G., Barker, D. M., and Huang, X.-Y.: A Description of the Advanced Research WRFModelVersion 4, Tech. rep., UCAR/NCAR [code/data set], https://doi.org/10.5065/1DFH-6P97, 2019.

Tan, Z., Lu, K., Hofzumahaus, A., Fuchs, H., Bohn, B., Holland, F., Liu, Y., Rohrer, F., Shao, M., Sun, K., Wu, Y., Zeng, L., Zhang, Y., Zou, Q., Kiendler-Scharr, A., Wahner, A., and Zhang, Y.: Experimental budgets of OH, HO_2, and RO_2 radicals and implications for ozone formation in the Pearl River Delta in China 2014, Atmos. Chem. Phys., 19, 7129–7150, https://doi.org/10.5194/acp-19-7129-2019, 2019.

Tan, Z., Lu, K., Ma, X., Chen, S., He, L., Huang, X., and Zhang, Y.: Multiple Impacts of Aerosols on O3 Production Are Largely Compensated: A Case Study Shenzhen, China, Environ. Sci. Technol., 56, 17569–17580, https://doi.org/10.1021/acs.est.2c06217, 2022.

Tonnesen, G. S. and Dennis, R. L.: Analysis of radical propagation efficiency to assess ozone sensitivity to hydrocarbons and NO_x: 2. Long-lived species as indicators of ozone concentration sensitivity, J. Geophys. Res., 105, 9227–9241, https://doi.org/10.1029/1999JD900372, 2000.

Wang, J., Zhang, Y., Xiao, S., Wu, Z., and Wang, X.: Ozone Formation at a Suburban Site in the Pearl River Delta Region, China: Role of Biogenic Volatile Organic Compounds, Atmosphere, 14, 609, https://doi.org/10.3390/atmos14040609, 2023.

Wang, T., Xue, L., Feng, Z., Dai, J., Zhang, Y., and Tan, Y.: Ground-level ozone pollution in China: a synthesis of recent findings on influencing factors and impacts, Environ. Res. Lett., 17, 063003, https://doi.org/10.1088/1748-9326/ac69fe, 2022.

Wang, W., van der A, R., Ding, J., van Weele, M., and Cheng, T.: Spatial and temporal changes of the ozone sensitivity in China based on satellite and ground-based observations, Atmos. Chem. Phys., 21, 7253–7269, https://doi.org/10.5194/acp-21-7253-2021, 2021.

Wang, W., Yuan, B., Peng, Y., Su, H., Cheng, Y., Yang, S., Wu, C., Qi, J., Bao, F., Huangfu, Y., Wang, C., Ye, C., Wang, Z., Wang, B., Wang, X., Song, W., Hu, W., Cheng, P., Zhu, M., Zheng, J., and Shao, M.: Direct observations indicate photodegradable oxygenated volatile organic compounds (OVOCs) as larger contributors to radicals and ozone production in the atmosphere, Atmos. Chem. Phys., 22, 4117–4128, https://doi.org/10.5194/acp-22-4117-2022, 2022.

Yang, G., Liu, Y., and Li, X.: Spatiotemporal distribution of ground-level ozone in China at a city level, Sci. Rep., 10, 7229, https://doi.org/10.1038/s41598-020-64111-3, 2020.

Yang, L. H., Jacob, D. J., Colombi, N. K., Zhai, S., Bates, K. H., Shah, V., Beaudry, E., Yantosca, R. M., Lin, H., Brewer, J. F., Chong, H., Travis, K. R., Crawford, J. H., Lamsal, L. N., Koo, J.-H., and Kim, J.: Tropospheric NO2 vertical profiles over South Korea and their relation to oxidant chemistry: implications for geostationary satellite retrievals and the observation of NO_2 diurnal variation from space, Atmos. Chem. Phys., 23, 2465–2481, https://doi.org/10.5194/acp-23-2465-2023, 2023.

Zaveri, R. A., Easter, R. C., Fast, J. D., and Peters, L. K.: Model for Simulating Aerosol Interactions and Chemistry (MOSAIC), J. Geophys. Res., 113, D13204, https://doi.org/10.1029/2007JD008782, 2008.

Zhang, Y., Dai, J., Li, Q., Chen, T., Mu, J., Brasseur, G., Wang, T., and Xue, L.: Biogenic volatile organic compounds enhance ozone production and complicate control efforts: Insights from long-term observations in Hong Kong, Atmos. Environ., 309, 119917, https://doi.org/10.1016/j.atmosenv.2023.119917, 2023.

Zhao, X., Zhou, W., and Han, L.: Human activities and urban air pollution in Chinese mega city: An insight of ozone weekend effect in Beijing, Phys. Chem. Earth Pt. A/B/C, 110, 109–116, https://doi.org/10.1016/j.pce.2018.11.005, 2019.

Zheng, B., Tong, D., Li, M., Liu, F., Hong, C., Geng, G., Li, H., Li, X., Peng, L., Qi, J., Yan, L., Zhang, Y., Zhao, H., Zheng, Y., He, K., and Zhang, Q.: Trends in China's anthropogenic emissions since 2010 as the consequence of clean air actions, Atmos. Chem. Phys., 18, 14095–14111, https://doi.org/10.5194/acp-18-14095-2018, 2018.

Zhu, S., Ma, J., Wang, S., Sun, S., Wang, P., and Zhang, H.: Shifts of formation regimes and increases of atmospheric oxidation led to ozone increase in North China Plain and Yangtze River Delta from 2016 to 2019, J. Geophys. Res.-Atmos., 128, e2022JD038373, https://doi.org/10.1029/2022JD038373, 2023.